Electronic Supplementary Material (ESI) for Reaction Chemistry & Engineering.
This journal is © The Royal Society of Chemistry 2021

Engineering Aspects of FlowNMR Spectroscopy Setups for Online Analysis of Solution-Phase Processes

Asad Saib,[a,b] Alejandro Bara-Estaún,[a,b] Owen J. Harper, [a,b,c] Daniel B. G. Berry, [a,b] Isabel A. Thomlinson, [a,b,c] Rachael Broomfield-Tagg, [a,b] John P. Lowe, [a,b] Catherine L. Lyall, [a,b] Ulrich Hintermair[a,b,c]*

[a] *Department of Chemistry, University of Bath, Claverton Down, BA2 7AY Bath, United Kingdom.*

[b] *Dynamic Reaction Monitoring Facility, University of Bath, Claverton Down, BA2 7AY Bath, United Kingdom.*

[c] *Centre for Sustainable & Circular Technologies, University of Bath, Bath BA2 7AY, United Kingdom.*

* *u.hintermair@bath.ac.uk*

Supplementary Information

Contents

1.0 Glossary

Name	**Description**
Back-mixing / dispersion	The mixing of liquid flowing through a pipe along the axis of travel by shear forces [laminar flow], eddies [turbulent flow], baffles, convection and/or molecular diffusion.
Back pressure regulator	A device that sustains a fixed pressure upstream of itself at its inlet, opening only when a set threshold has been reached (either by releasing a spring-loaded valve or rupture of a bursting disk).
Bodenstein number	Ratio of how much substance is introduced from convection versus diffusion. Used to quantify the amount of back-mixing in liquids flowing through a cylindrical pipe.
Cavitation	Process of unwanted gas or vapour bubble formation in liquids inside a positive displacement pump due to the suction pressure created by the pump exceeding gas solubility or vapour pressure of the liquid.
Check valves	A valve that only allows the movement of a fluid in one direction.
Closed-loop setup	Piping set up that does not allow sample to be exposed to the environment.
Continuous stirred-tank reactor (CSTR)	A reaction vessel equipped with an impeller or other active mixing device.
Dead volume	Internal volume of flow devices not uniformly reached by flow: total volume = swept volume + dead volume
Dynamic viscosity	Tangential force per unit area required to move a fluid at a unit velocity. Described by the Shear stress, τ (N/m^2) over the shear rate γ (s^{-1}) as $\mu = \tau / \gamma$
Elongation at break	Ratio of starting length of a material versus the length at break when pulled in one direction.
Flow velocity	Volume of fluid passing through a cross sectional area per unit time: $Q = V / t$ Q = Flow rate/velocity, V = Volume of fluid, t = Time
Gaussian	A bell-shaped curve whereby measurement values are equally above and below the mean value.
GxP	A term utilised to refer to a collection of quality guidelines. ‘’x’’ can stand for various fields

Heat transfer fluid / thermofluid	Fluid mixture used to transport heat into or out of a system by flowing in close contact with the container. If used to heat or cool another non-stationary liquid inside the container it may be used in concurrent flow or counter-flow mode (depending on whether the rate of heat exchange or sample exit temperature is more important).
Hydrostatic pressure	The pressure that a non-compressible fluid exerts in a container.
Impact strength	The resistance of a material to fracture by a blow, expressed in terms of the amount of energy absorbed before fracture. Measured by impact energy (J or ft-lb) divided by the material thickness (m or in).
Internal volume	Volume of fluid inside a container. For cylindrical tubing: $V = \pi r^2 l$ where V = volume of fluid, r = internal radius of tubing, l = length of tubing.
Laminar flow	Non-turbulent movement of fluid through a confinement (e.g. cylindrical tubing).
Mechanical stress	Physical forces felt on a material during use.
Mean (hydrodynamic) residence time	The residence time of a set of parcels that is quantified in terms of the frequency distribution of the residence time: τ = volume / volumetric flow rate.
Modulus of Elasticity	The measure of an object's or substance's resistance to being deformed elastically when stress is applied. Elastic modulus, λ = stress (Pa) / strain
Net positive inlet pressure (NPIP)	Sample inlet pressure required to avoid cavitation during the suction phase of a pump.
Outgassing	Process whereby a material releases gas upon exposure to a certain level of heat or vacuum.
PID controller	A control mechanism based on a feedback loop used to regulate process variables to a target value with control over responsiveness (proportional term), steadiness (integral term) and sensitivity (derivative term).
Plug flow	A model of perfect fluid flow. Ideal plug flow means the entire fluid front is moving at the exact same velocity throughout and there is no back mixing due to shearing or diffusion.
Positive displacement	Operates by repeatedly enclosing a small volume of liquid and

pump	moving it mechanically from the suction side to the discharge side, intercepting the liquid stream temporarily with each cycle.
Pressure drop / flow resistance	Pressure difference across two points in a fluid moving through a confinement caused by frictional forces.
Priming	Process of filling the internal volume of a pump entirely with incompressible liquid.
Pump head	Maximum height with which a pump can move fluid against gravity.
Push-fit connection	A type of lose tubing connection that can be affected without tools.
Residence time distribution (RTD)	Probability distribution of the time a fluid spends in a flow system.
Reynold's number	Ratio of inertial forces to viscous forces within a fluid moving through a confinement. Used to determine whether a flow is laminar (Re <3000) or turbulent (Re >3000).
Slippage	An uncontrolled movement of fluid through a pumping mechanism, flow valve or back-pressure regulator.
Stroke velocity	Speed at which a round of the pump's mechanism is completed.
Suction pressure	Pressure drop felt at the section of tubing between the sample reservoir and the pump inlet.
Swept volume	Volume of fluid moved by one stroke of the pump.
Tailing	Broadening of a normal distribution RTD curve to longer residence times due to dead volumes within the system.
Temporal resolution	Discrete resolution of a measurement with respect to time.
Tensile strength	Resistance of a material to breaking under tension relative to its cross-sectional area.
Thermal expansion coefficient	Describes how a material expands geometrically due to change in temperature.
Umbilical	Non-rigid main body of flow tube used to deliver reaction mixture to tube head/flow tip and back. Often includes thermofluid and temperature sensors as well as insulating foam and bending protectors.
Vessel number	*n* of a cascade of small, ideal CSTRs that may be used to model a flow setup
Viscosity limit	A measure of a fluids resistance to distortion at specified rates.

2.0 General

Unless otherwise stated, all manipulations were carried out under an open-air atmosphere. Acetone, toluene and *n*-hexane were purchased from Fisher Chemicals solvents in HPLC grade, with 99.9% purity. Fluorescein was purchased from Sigma-Aldrich and used without further purification. Carbon monoxide (99.99%), carbon dioxide (99.99%), hydrogen (99.95%) and a mixture of argon (90%) with hydrogen (10%) were supplied by BOC. All solvents were passed through 0.2 µm syringe filters (VWR 514-0070) prior to flowing through the flow path.

High pressure experiments were carried out in a 100 mL Büchi Miniclave pressure reactor, which was connected to the FlowNMR apparatus *via* 1/16" Swagelok connections. Experiments carried out under atmospheric conditions were done using round-bottomed glass flasks, connected to the FlowNMR apparatus *via* rubber septa.

For all experiments performed, one of the seven following pumps was used to circulate mixtures through the flow setup:

- Vapourtec SF-10[1] (Peristaltic pump)
- Knauer Azura P4.1S[2] (Double-piston pump)
- HNP Mikrosysteme GmbH Mzr-6355 [3] (Annular gear pump)
- HNP Mikrosysteme GmbH Mzr-2921X1-hs-vb[4] (Mini annular gear pump)
- Tacmina QI-10-6T[5] (diaphragm pump)
- Cole-Parmer Masterflex 74900-05[6] (syringe pump)
- Vici M6 HP[7] (rotary tetra-piston pump)

NMR spectra were recorded on a Bruker Ultrashield 500 MHz Avance III HD equipped with a room temperature BBO probe or BBFO probe. NMR data processing was performed with TopSpin 4.0.6 and Dynamics Center 2.5.6. UV-visible spectroscopic data was collected using an Ocean Optics fibre-optic setup consisting of a deuterium-halogen light source (DH-2000-BAL) connected to a 0.5 cm lensed PEEK SMA-Z flow cell and a QEPro spectrometer (10 µm slit) *via* SMA-terminated 400 µm solarisation-resistant light guides. OceanView 1.6.5 software was used for continuous spectral acquisition from 200 – 1000 nm resolution with an integration time of 10 ms and averaging 100 scans.

The flow rate was measured by a Digital Mass Flow Meter from Bronkhorst (Cori-flow Mini M13). The pressure in the flow path was recorded using two custom-made pressure sensors from DJ instruments (DJ Instruments DF2-TI-01- 500-5V). The pressure in the autoclave reactor was measured by a QuickStart pressure gauge from IDEX Health & Science. Both flowmeter and custom-made pressure sensor software was installed and interfaced to a LabVIEW VI for easier control, data visualization and logging. Data processing was done using Microsoft Excel and/or Origin 2017.

3.0 FlowNMR Apparatus

The FlowNMR apparatus depicted below (Figure S1) consisted of 3 main components, the reaction vessel (highlighted in red by heat exchanger 3), the flow path (highlighted in yellow by heat exchanger 1) and the flow tube (highlighted in blue by heat exchanger 2). The flow path was composed of varying sizes of polyetheretherketone tubing (PEEK, OD 1/16”, ID 0.51/0.76/1.02 mm, Upchurch Scientific), which connected the reaction vessel to the UV-Visible flow cell (PEEK SMA-Z, Ocean Optics) and InsightMR flow tube (Bruker). The InsightMR flow tube consisted of PEEK (OD 1/32”, ID 0.51 mm, Upchurch Scientific) transfer lines housed within concentrically aligned Teflon tubing that connects to the flow tip (Figure S1). The chosen pump was connected to the FlowNMR apparatus *via* polyetheretherketone (PEEK, O.D 1/16”, I.D 0.76 mm, Upchurch Scientific) tubing. For the gas permeability experiments, either PEEK or polytetrafluoroethylene (PTFE, OD 1/16”, ID 0.76 mm, Upchurch Scientific) tubing was used. Connections to reaction vessels were secured *via* rubber septa, HPLC-type (1/16”) or Swagelok (1/16”) fittings. Thermal regulation of the flow path and flow tube was maintained by 2 heat exchangers (Julabo CORIO CD-300F, thermofluid – 50:50 ethylene glycol:water). Thermal regulation of the reaction vessel was controlled by either a heat exchanger (Julabo CORIO CD-300F, thermofluid – 50:50 ethylene glycol: water) connected to a reactor jacket (DrySyn Snowstorm ONE) or a hotplate (IKA RCT B S002) with a reactor jacket (paraffin oil bath).

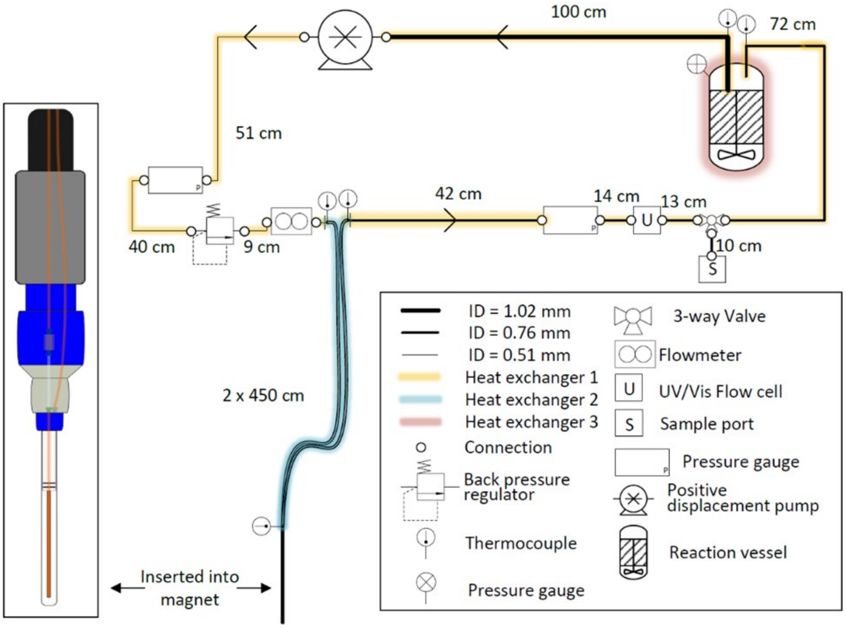

Figure S1: P&ID schematic of a closed-loop recirculating FlowNMR setup with exemplary length scales, tubing ID (indicated by the line thickness), and indication of sequential temperature control by use of these independent heat exchangers (colour coding).

4.0 Methods

4.1 Gas permeability tests

A QuickStart pressure sensor (IDEX health & Science) was attached to a 100 mL Büchi Miniclave pressure reactor *via* a 20 cm of PEEK tubing (OD 1/16", ID 0.76 mm). The appropriate flow tube threaded with either PEEK or PTFE (OD 1/32", ID 0.51 mm) was connected and the polymer tubing (PEEK/PTFE, OD 1/16", ID 0.76 mm) used in the flow path was changed to match. The FlowNMR apparatus was flushed and filled with toluene (4 mL/min) for 20 minutes to remove residual storage solvent. Toluene (15 mL) and a Teflon-coated stirrer bar were charged to the pressure reactor, which was then sealed and checked for leaks. Data acquisition was started, and solvent was recirculated by the annular gear pump (HNP Mikrosysteme GmbH Mzr-6355, 4 mL/min). The autoclave was then pressurised with 10 bar of either H_2, CO or CO_2 and monitored for 4 hours. A control experiment was carried out monitoring 10 bar of H_2 in the autoclave reactor without connecting the flow path to ensure observed pressure losses were due to tubing material used (See Figure S2).

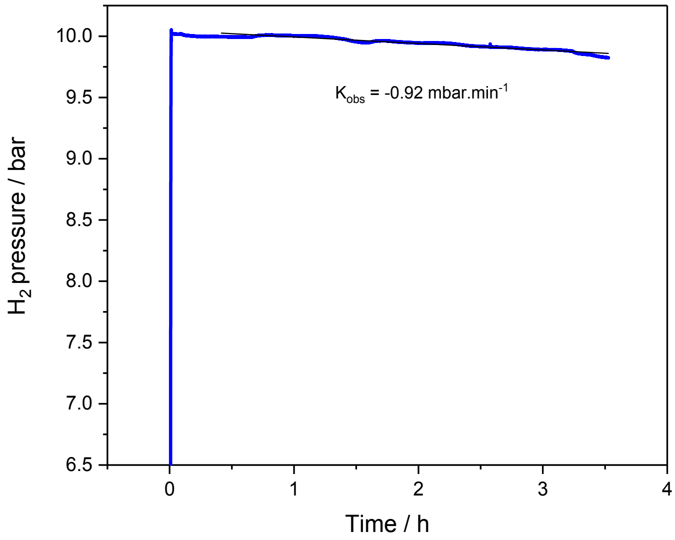

Figure S2: Headspace pressure and gas loss rate of H_2 of a Büchi Miniclave pressure reactor containing toluene (15 mL) that was not attached to the FlowNMR apparatus. K_{Obs} -0.92 mbar/min (Reactor) in comparison to -1.43 mbar/min (peek) and -5.69 mbar/min (PTFE).

4.2 Pump testing under pressure

A Cori-flow Mini M13 (Bronkhorst) flow meter was inserted into the flow path and the FlowNMR apparatus was flushed and filled with toluene (4 mL/min) for 20 minutes to remove residual solvent. Toluene (15 mL) and a Teflon-coated stirrer bar were charged to the pressure reactor, which was then sealed, checked for leaks and connected to the FlowNMR apparatus in a recirculating setup. Pressure and flow rate data acquisition was started, and the relevant pump (either the peristaltic, double-piston, annular gear, rotating-tetra piston or diaphragm pump) was set to 4 mL/min, heat exchanger 1, 2, the probe and the hotplate were set to 50 °C and allowed to equilibrate. The reactor was increasingly pressurised to 5, 10 and 20 bar at 20 minute intervals. The reactor was then vented, re-pressurised to 10 bar and left for another 20 minutes to check pressure performance after being pressurised and depressurised.

4.3 RTD experiments for FlowNMR apparatus

The UV flow cell (PEEK SMA-Z, Ocean Optics) was inserted at the end of the flow path (see Figure S1) and the deuterium-halogen light source (DH-2000-BAL) was turned on and allowed to warm up for a minimum of 30 minutes. The FlowNMR apparatus was flushed and filled with acetone (4 mL/min) for 20 minutes to remove any residual solvent. A solution of fluorescein in acetone (500 mL, 12 mM) was charged to a round-bottomed flask and connected to the FlowNMR apparatus *via* a rubber septa with the outlet connected to a waste bottle. UV-vis data acquisition and the pump were turned on simultaneously and data was acquired until the flow path was uniformly filled with fluorescein solution (Fill). The pump was stopped, the inlet was placed in acetone and acquisition and flow were started simultaneously, data was recorded until the flow path was uniformly emptied of fluorescein solution (Empty). The change in the absorbance of fluorescein (334 nm) was used to determine whether the flow path had been uniformly emptied/filled. This was repeated for all of the aforementioned pumps at 1–6 mL/min. Residence time distribution profiles were obtained for all pumps using the empty profile (see section 10.1).

4.4 Measurement of pump pulsation

A round bottomed flask was connected to the pump and flow meter (Cori-flow Mini, Bronkhorst) in a recirculating setup with PEEK tubing (Length 50 cm, O.D 1/16”, I.D 0.51 mm). The FlowNMR apparatus was flushed and filled with acetone (4 mL/min) for 15 minutes to remove residual storage solvent. Toluene (15 mL) was charged to the flask and both flow and data acquisition were started (0.2 s intervals). This was repeated for each pump at flow rates of 2, 3 and 4 mL/min for 5 minutes each.

4.5 Pulsation and NMR spectroscopy

The FlowNMR apparatus was flushed and filled with acetone (4 mL/min) for 20 minutes to remove residual storage solvent. Acetone (100 mL) was charged to a round bottom flask and connected to the flow apparatus inlet, with the outlet in the waste bottle. The FlowNMR tube was placed in the spectrometer. Data acquisition and flow were started, and the acetone integral was monitored every 0.4 s for 5 minutes. The experiments were performed at 2, 4 and 6 mL/min with each of the peristaltic, annular gear and diaphragm pumps.

NMR parameters: ^{1}H, PULPROG (zg2d), ns = 1, d1 = 0.01 s, d20 = 0.25 s, O1p = 6.175, SW = 20, TD = 1200

4.6 RTD experiments to FlowNMR tip

The FlowNMR apparatus was flushed and filled with acetone (4 mL/min) for 20 minutes to remove residual storage solvent. Hexane (15 mL) was added to a round-bottomed flask and connected to the inlet of the FlowNMR apparatus with the outlet in the waste bottle. The FlowNMR tube was placed in the spectrometer. NMR data acquisition and the pump were turned on simultaneously and data was acquired until the flow path was uniformly filled with hexane (Fill). The pump was stopped, the inlet tubing was placed in acetone and acquisition and flow were started simultaneously; data was recorded until the flow path was uniformly emptied of hexane (Empty). The change in acetone integral was used to determine whether the flow path (to the tip) had been uniformly filled/emptied. Residence time distribution profiles were obtained for the peristaltic pump at 2, 4 or 6 mL/min using the empty profile of acetone (see section S4.).

NMR parameters: ^{1}H, PULPROG (zg2d), ns = 1, d1 = 0.01 s, d20 = 0.4 s, O1p = 6.175, SW = 20, TD = 1024

5.0 Tubing

Table S1: Typical Chemical compatibility chart for common tubing polymers[8]

Resistance at 20°C	**PEEK**	**FEP**	**PFA**	**PTFE**
Acetone	A	A	A	A
Ammonia (liquid)	B	A	A	-
Benzene	A	A	A	-
Ethanol	A	A	A	A
Isopropyl ether	-	A	A	A
Nitric acid (100%)	C	A	A	A
Perchloric acid	A	B	B	A
Tetrahydrofuran	B	A	A	A
Toluene	A	A	A	A
Water	A	A	A	A

A = suitable
B = marginal; dependent on application
C = not recommended
– = no data available

6.0 Injection Capillary

The connections to the fused silica capillary were made for ease of tip replacement and flow tube repair - details of the fittings and parts for this modification can be seen below in Figure S3 and S4. The silica capillary is connected to the body of the flow tube via a push-fit connection with a polymer sleeve (1/16” FEP) that is secured in a 1/16” compression fitting. This other end of the sleeve is then connected to the transfer line via UNF 6-40 flat unions and fittings, which can be used for both 1/16” and 1/32” tubing sizes.

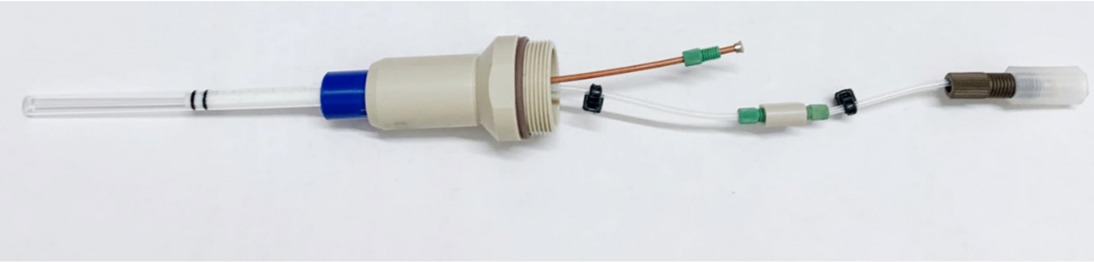

Figure S3: Image of removed flow tip (silica capillary) with external connections visible.

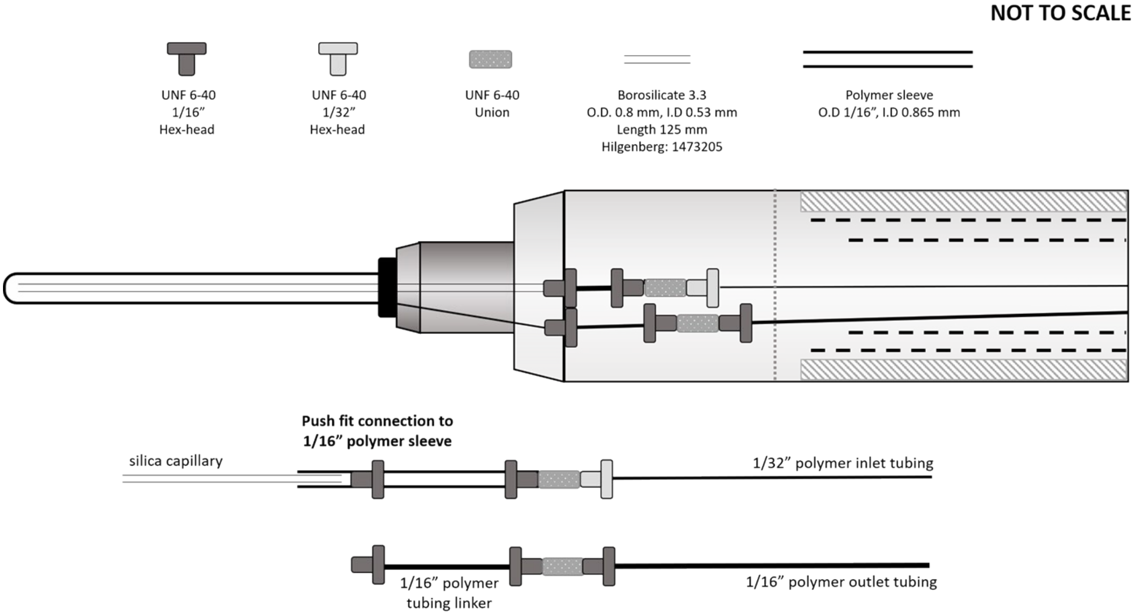

Figure S4: Schematic of connections made in the flow tip (silica capillary) with material details highlighted.

7.0 Volumes, internal diameters, and the importance of pressure drop

Original form of the Darcy-Weisbach equation and derivation:[9]

$$\Delta p(Pa) = \frac{128 \cdot \ Q(m^3/s) \ \cdot \eta(Pas)}{\pi} \sum \frac{L(m)}{D_c^4(m)}$$

Equation S1

This equation is converted to different units by using the following conversions:

(**Δp**) 1 Pa = 0.01 mbar, (**Q**) 1 m^3/s = 6 x 10^7 $mLmin^{-1}$, (**η**) 1 Pas = 1000 mPas, (**L** / **D$_c$**) 1 m = 1000 mm

Which are inserted into the original equation:

$$\frac{1[Pa]}{0.01[mPa]} = \frac{128 \cdot \ 1[m^3/s] \ \cdot 1[Pas]}{\pi \cdot 6 \times 10^7 [mLmin^{-1}] \cdot 1000[mPas]} \sum \frac{\left(\frac{1[m]}{1000[mm]}\right)}{\left(\frac{1_c[m]}{1000[mm]}\right)^4}$$

Equation S2

This calculation gives a value of roughly 1/147.26 as seen below:

$$\left(\frac{128}{\pi}\right) \cdot \left(\frac{1}{6 \times 10^7}\right) \cdot \left(\frac{1}{1000}\right) \cdot \frac{\left(\frac{1}{1000}\right)}{\left(\frac{1}{1000}\right)^4} \cdot 0.01 = 0.00679061 \ldots \approx \frac{1}{147.26}$$

Equation S3

Therefore, the final equation with desired units is as follows:

$$\Delta p[Pa] = \frac{128 \cdot \ Q\left[\frac{m^3}{s}\right] \cdot \eta[Pas]}{\pi} \sum \frac{L[m]}{D_c^4[m]} \approx \Delta p[mbar] = \frac{Q[mLmin^{-1}] \ \cdot \eta[mPas]}{147.26} \sum \frac{L[mm]}{D_c^4[mm]}$$

Equation S4

A summary of all these terms and their units can be found below in Table S2:

Table S2: Parameters in the Darcy-Weisbach equation and units used in both forms.

Symbol	**Name**	**Original Unit**	**Converted Unit**
Δp	Flow resistance in a pipe/tube	Pa	mbar
Q	Flow rate	m^3/s	mL/min
η	Dynamic viscosity of fluid	Pas	mPas
L	Pipe/tubing length	m	mm
D_c	Internal diameter of a circular pipe/tubing	m	mm

Table S3: Calculated suction pressure of water and ethanol for 100 cm tubing with 1 mm ID from 4 - 28 °C compared to solvent vapour pressure at the same temperature.

Solvent	**Temperature / °C**	**Vapour pressure / bar**	**Suction pressure for 100 cm, 1 mm ID tubing / bar**
Water	4	0.00807	0.04266
	8	0.01066	0.03713
	12	0.01395	0.03329
	16	0.01810	0.03001
	20	0.02330	0.02721
	24	0.02974	0.02479
	28	0.03769	0.02268
Ethanol	4	0.02076	0.04490
	8	0.02722	0.04109
	12	0.03537	0.03768
	16	0.04558	0.03462
	20	0.05826	0.03187
	24	0.07390	0.02939
	28	0.09304	0.02715

8.0 Velocity Imaging

A solution of chromium(III) 2,4-pentanedionate (2.0 mg, 0.57 mM) in chloroform (9.5 mL $CDCl_3$ and 0.5 mL $CHCl_3$, total 10.0 mL) was circulated through the flow system using a peristaltic pump (Vapourtec SF-10). Velocity imaging experiments were carried out at seven flowrates from 0.0 to 4.0 mL min^{-1} using the sequence in Figure S5 described by Morris.[10] A diffusion delay, Δ, of 0.08 s was used, with 29 diffusion delay imbalance times, $\Delta\Delta$. These ranged from −0.07 and +0.07 s and included a greater density of data points at the centre of the distribution (small $\Delta\Delta$). Eight scans were used for each value of $\Delta\Delta$, and p30 was set to 1000 µs.

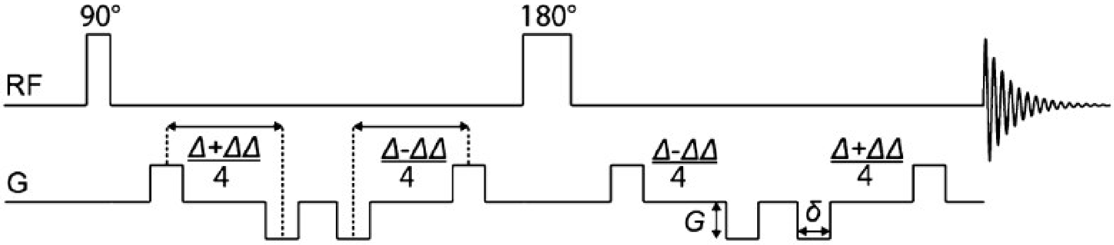

Figure S5*:* From Swan *et al.*[10] When the diffusion delay imbalance ΔΔ = 0, the pulse sequence is equivalent to a convection compensated DOSY experiment.

The maximum velocity at each flowrate was determined by curve fitting (Figure S6). For each flowrate, peak integrals at different diffusion delay imbalance values, $\Delta\Delta$, were exported and fit to Equation S5 using a nonlinear least squares fit in MS Excel. A_G is the gradient pulse shape factor, S_0 is the maximum signal amplitude, and γ is the gyromagnetic ratio. The result of the curve fit gives v_{max}, the values of which are shown in Figure S6 as a function of volumetric flow rate.

$$F(\Delta\Delta) = \frac{S_0 \sin(\gamma\delta G A_G v_{max}\Delta\Delta)}{\gamma\delta G A_G v_{max}\Delta\Delta}$$

Equation S5

4.0 mL min^{-1}

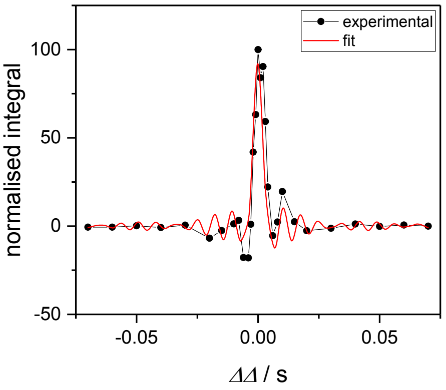

1.0 mL min^{-1}

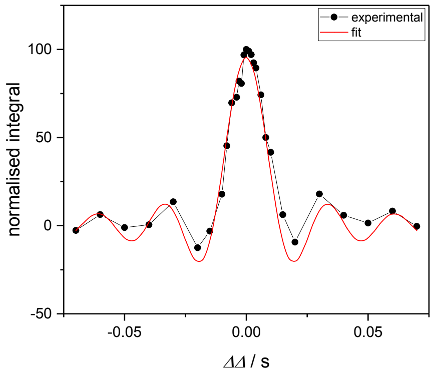

0.5 mL min^{-1} 0.3 mL min^{-1}

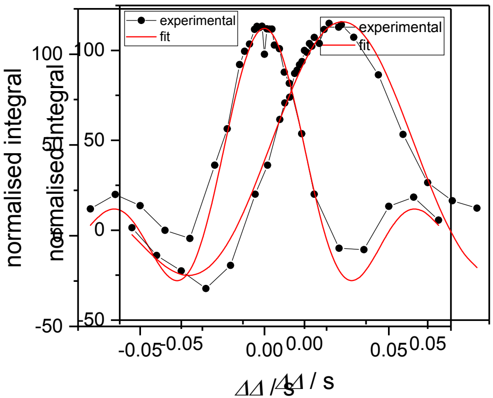

0.2 mL min^{-1}

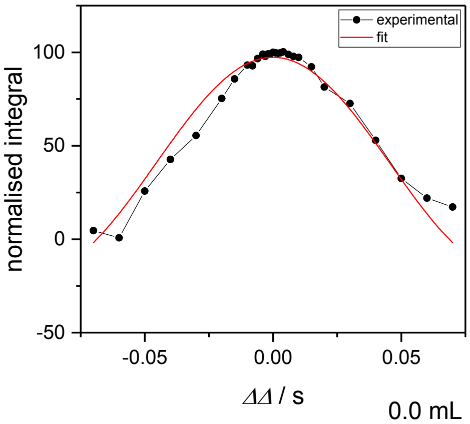

0.1 mL min^{-1}

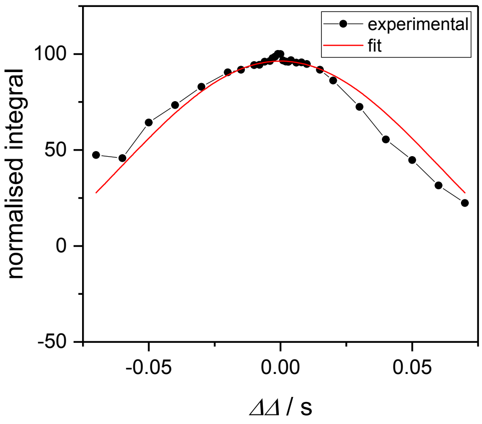

0.0 mL min^{-1}

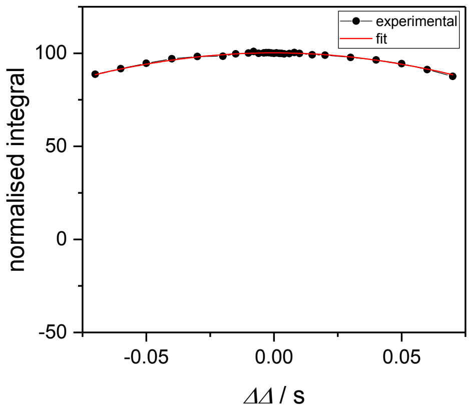

Figure S6: Experimental signal intensity as a function of variable delay ΔΔ for all seven flow rates, along with curve fits to Equation S23 used to obtain v_{max} values.

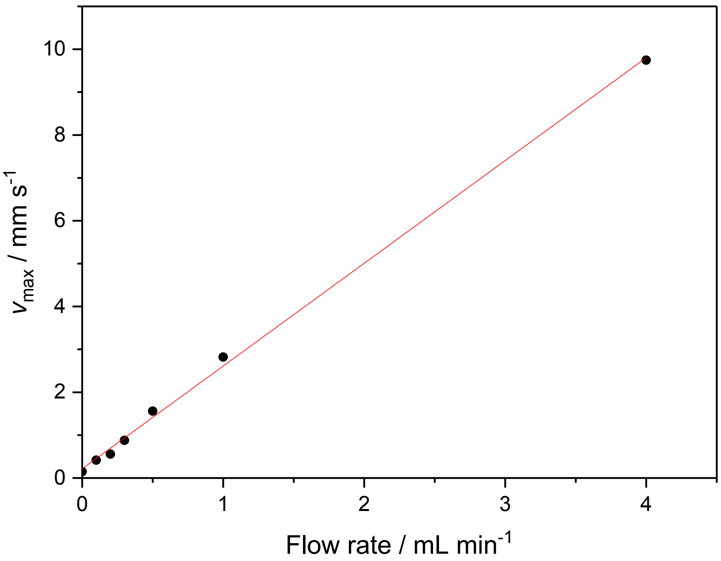

Figure S7: Correlation of maximum velocity calculated from ΔΔ fitting with volumetric flow rates from the peristaltic pump.

9.0 Temperature

9.1 Heat Transfer Model

Heat transfer in the system was modelled on conduction through a pipe wall combined with volumetric flow rate in a heating system (see Figure S8).[11-14] Equation S5 calculates heat conduction through a pipe wall where Q is heat flow (W), k is the overall heat transfer coefficient of the system (W/m^2.K), A is the surface area of heat flow (outer tubing surface, m^2) and ΔT is the temperature difference between the solvent temperature (T_{solv}) and external temperature(T_{ext}) (K).

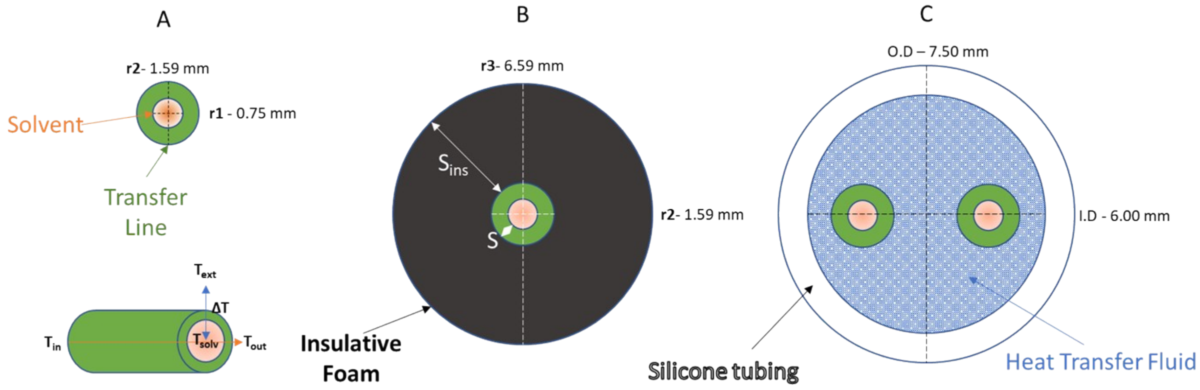

Figure S8: Cross-sectional diagram of heat transfer modes for no heat regulation (A), passive heat regulation (B) and active heat regulation (C). Models use 1/16" PEEK tubing, insulative foam and general-purpose silicone tubing filled with a 50:50 ethylene glycol / water mixture. Material dimensions used in equations are labelled.

$$\dot{Q} = kA\Delta T$$

Equation S6

Equation S7 is used for determining the surface area of a cylinder (outer tubing surface) where r is the radius of the pipe and L is the length of the tubing.

$$A = 2\pi rL$$

Equation S7

Equation S8 defines the overall heat transfer coefficient of the system which is a sum of the resistances to heat transfer where α is the heat transfer coefficient of a component (W/m^2.K), λ is the thermal conductivity of a component (W/m.K), S is the wall thickness (m) and r1/r2 are the radii of the inner and outer pipe walls respectively (m).

$$k = \frac{1}{\frac{1}{\alpha 1} + \frac{S}{\lambda} ln \frac{r2}{r1} + \frac{r1}{a2r2}}$$

Resistance term for solvent inside tubing

Resistance term for tubing material

Resistance term for surrounding liquid or gas

Equation S8

For model 2, which includes the addition of an insulative material, another term is added for the thermal resistance of the insulation material (Equation S9), where λ_{ins} is the thermal conductivity of a component (W/m.K), S_{ins} is the wall thickness of the insulation material (m) and r3 is the outer radius of the insulation material (m).

$$k = \frac{1}{\frac{1}{\alpha 1} + \frac{S_{ins}}{\lambda_{ins}} ln \frac{r3}{r2} + \frac{S}{\lambda} ln \frac{r2}{r1} + \frac{r1}{a2r2}}$$

Equation S9

Equation S10 calculates the heat transfer coefficient (α, $W/m^2.K$) for a flowing liquid where Nu is the Nusselt number (assumed to be 3.66 in the case of laminar flow with a uniform outer wall temperature),[13] λ is the thermal conductivity of the liquid (W/m.K) and D is the diameter of the tubing (inner wall, m^2).

$$\alpha = Nu \times \frac{\lambda}{D}$$

Equation S10

Equation S11 defines the volumetric flowrate for a heated system[15] where V is the volumetric flowrate (m^3/s), Q is the heat flow (kW), C_p is the heat capacity of the solvent (kJ/kg.K), ρ is the density of the solvent (kg/m^3), T_{in} and T_{out} are the inlet and outlet temperature of the tubing respectively (K).

$$\dot{V} = \frac{\dot{Q}}{C_p \rho (T_{in} - T_{out})}$$

Equation S11

Equation S11 is then rearranged to make the outlet temperature the subject in Equation S12.

$$T_{out} = T_{in} - \frac{\dot{Q}}{C_p \rho \dot{V}}$$

Equation S12

By substituting kAΔT for Q we achieve a single calculation for the outlet temperature including all variables, in Equation S13. A summary of all of these terms and their units can be found beneath in Table S4.

$$T_{out} = T_{in} - \frac{kA\Delta T}{C_p \rho \dot{V}}$$

Equation S13

Table S4: Summary of terms with units used.

Symbol	**Name**	**Unit**
Q	Heat flow	W
k	Overall heat transfer coefficient	$W/m^2.K$
A	outer surface of tubing	m^2
ΔT	Temperature difference ($T_{solv} – T_{ext}$)	K
λ	Thermal conductivity (component)	W/m.K
L	Length	m
r	Radius	m
α	Heat transfer coefficient (component)	$W/m^2.K$
Nu	Nusselt Number	None
D	Diameter	m^2
S	Wall thickness	m
C_p	Heat capacity of solvent	kJ/kg.K
$\dot{V}$	Volumetric flowrate	m^3/s
ρ	Density	kg/m^3

Now we have achieved the outlet temperature for a length of tubing we must define the length of tubing we want to study. In order to achieve a temperature profile that asymptotically approaches the target temperature we must perform the calculation over short lengths, with the T_{in} of an increment being equal to the T_{out} of the previous increment. This is then iterated to the desired length to create a temperature profile. Varying the size of the length increment had little effect on the magnitude of heat loss observed in the temperature profile (Figure S9). Length values for plots throughout the study use 1.0 cm increments.

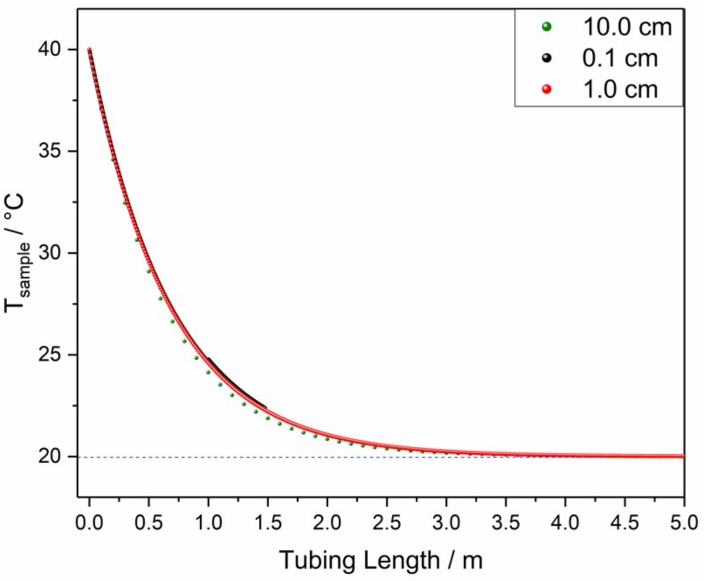

Figure S9: Modelled temperature gradient between water (313 K) and room temperature (293 K) using different sized increments of length in Equation S9. Modelled conditions: 4 mL/min, 1/16" PEEK tubing, α_{air} = 35.

It is noted that the heat transfer coefficient for air (α_{air}) can vary greatly due to many factors and its flow is not always easily characterizable. From Table S5 we can estimate that the alpha will be between 10 and 100 W/m^2.K. The effect of this value on the overall temperature gradient can be seen in Figure S10.

Table S5: Typical values of heat transfer coefficient (α) under different conditions.[11]

Flow Type	**A / Wm^{-2}K^{-1}**
Low speed of air over a surface	10
Moderate speed flow of air over a surface (>50 m/s)	100
Moderate speed cross-flow of air over a cylinder	200
Moderate flow of water in a pipe	3000
Boiling water in a pipe	50000
Free convection of air over a plate with a 30°C temperature difference	5

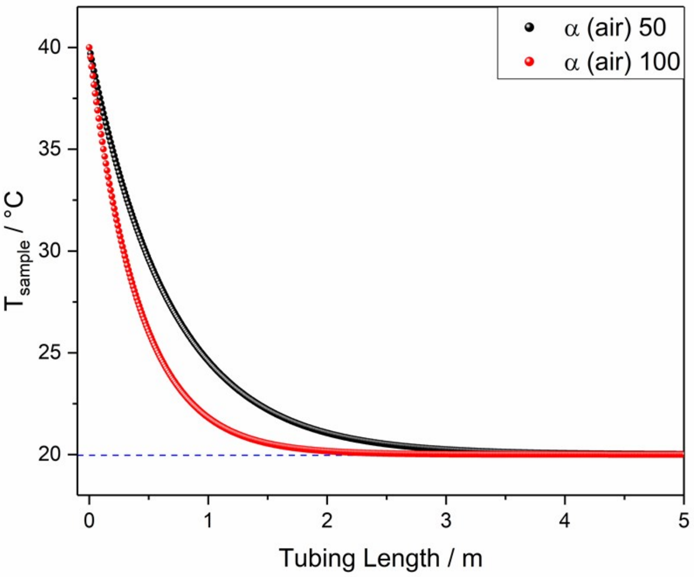

Figure S10: Modelled temperature gradient between water (313 K) and room temperature (293 K) using different heat transfer coefficients for air (α_{air}). Modelled conditions: 4 mL/min, 1/16" PEEK tubing.

To determine the most appropriate α_{air} for the system studied an experiment was carried out under the same conditions at different tubing length to achieve a temperature gradient over length. This curve was then compared to calculation and the optimal heat transfer coefficient was selected.

Figure S11 below shows a plot comparing active heat regulation and no heat regulation when the temperature gradients are the same (40 °C to 20°C). Active heat regulation as expected would more efficiently cool a reaction mixture than just exposing it to a low flow of air. If cooling a reaction mixture down for analysis (or to prevent thermal runaway) the reaction solution without regulation might not fully cool down prior to detection if using a 4 m long flow tube.

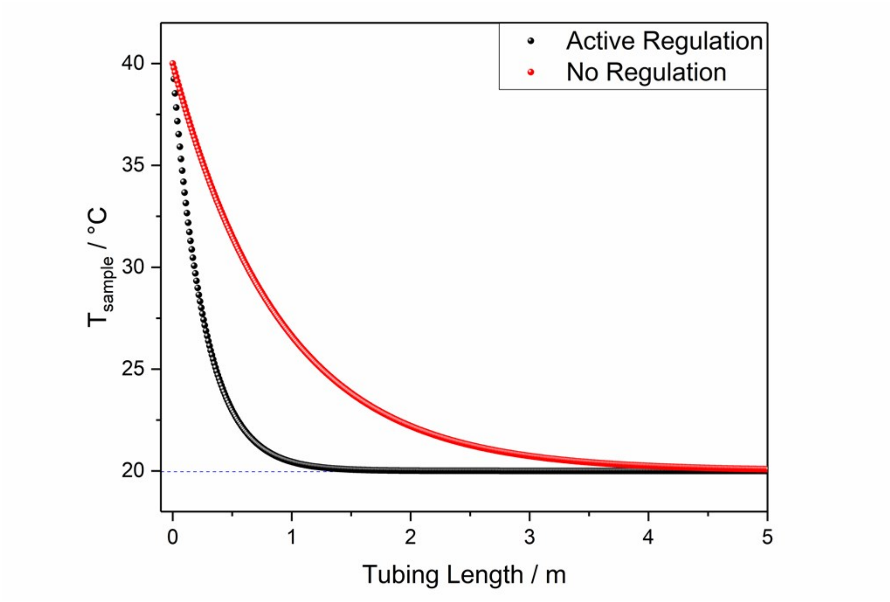

Figure S11: Modelled temperature loss between water (40 °C) when actively cooled to 20 °C by a heat exchanger (black) or passively cooled by ambient temperature (red). Dotted line indicates room temperature (blue). Modelled conditions: 4 mL/min, 1/16” PEEK, 7.5 mm O.D silicone tubing, 50:50 ethylene glycol: water thermofluid.

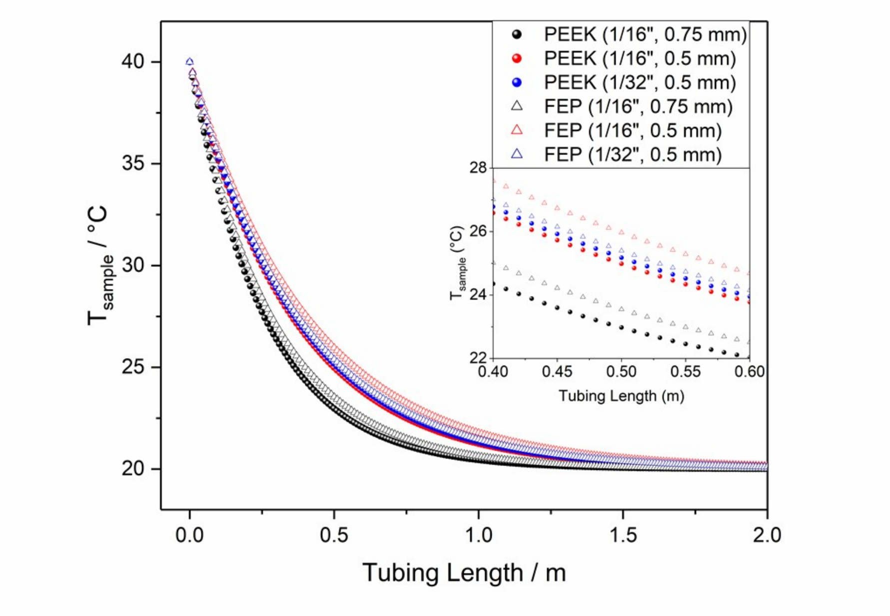

Figure S12: Modelled temperature loss between water (40 °C) when actively cooled to 20 °C by a heat exchanger for PEEK and FEP tubing of varying outer and inner diameter. Modelled conditions: 4 mL/min, 7.5 mm O.D silicone tubing, 50:50 ethylene glycol / water thermofluid.

In all the heat transfer models in this study the following assumptions are made:

- The flow within the transfer line is classified as laminar.
- The outside temperature is uniform (room temperature or uniformly heated transfer fluid).
- Insulative foam used for passive insulation has the same heat transfer properties as Armaflex™ insulation.[16]
- The heat transfer coefficient of air (α_{air}) is 35 as estimated by experiment (SX.X)

A summary of all tubing and solvents studied and their physical properties used in the model can be found below in table S6.

Table S6: Table of physical properties of the tubing materials and solvents used in the heat transfer model. a – 50:50 mixture, values at 40°C.

Material	**Thermal Conductivity / λ @ 25 °C**	**Inner diameter / mm**	**Outer diameter / mm**
PEEK 1/16”[17]	0.25	0.75	1.59
PEEK 1/32”	0.25	0.50	0.79
FEP 1/16”[18]	0.21	0.75	1.59
FEP 1/32”	0.21	0.50	0.79
Armaflex[16]	0.042	1.59	2.59
Solvent[19]	**Thermal Conductivity / λ @ 25 °C**	**Density / $g.mL^{-1}$**	**Heat Capacity $J.g^{-1}.K^{-1}$**
Water	0.598	0.997	4.18
Methanol	0.200	0.791	2.53
Acetone	0.161	0.790	2.17
Dichloromethane	0.122	1.327	1.19
Toluene	0.131	0.867	1.71
Hexane	0.120	0.655	2.27
Ethylene glycol: Water[a] [20, 21]	0.398	1.069	3.34

9.2 Thermal Model Validation

A stirred 1 L reservoir of water was heated to 40 °C by a hotplate, 1.42 m of polyetheretherketone tubing (PEEK, OD 1/16”, ID 0.76 mm) connected to a Vapourtec SF-10 peristaltic pump was inserted into the reservoir, secured with a rubber septum. Thermocouples were positioned in the heating block, reservoir, and tubing exit. The water was flowed directly onto the thermocouple and was allowed to come to thermal equilibrium for 20 minutes. Single point readings were taken and the tubing was progressively cut to shorten the total path length (Table S7, Figure S12). 10 cm was added to the overall length to account for the tubing within the peristaltic pump. For simplicity this was assumed to have similar heat transfer properties to the PEEK tubing (Figure S13 – Thermal Image).

Table S7: Table of exit thermocouple reading (K) against total tubing length (m) of water (313 K) being flowed at 4 mL/min by a Vapourtec SF-10 peristaltic pump through 1/16” OD PEEK tubing.

Tubing Length / m	**Measured Exit Temperature / K**
1.420	295.83
1.335	296.13
1.135	297.03
1.050	297.53
0.940	298.43
0.865	298.93
0.730	300.13
0.635	301.03

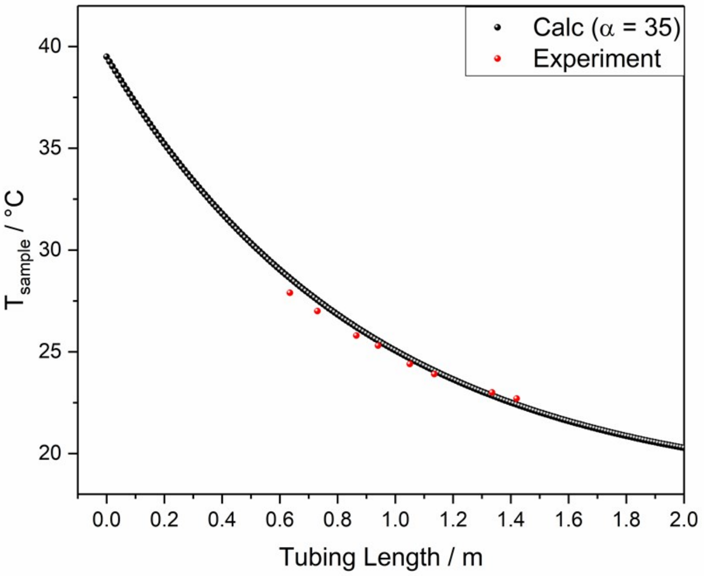

Figure S13: Calculated (black) versus experimental (red) data for the temperature loss between water (313 K) and room temperature (293K). Conditions: 4 mL/min, 1/16” tubing.

Using a heat transfer coefficient (α_{air}) of 35 resulted in the best fit with experimental data and as such this was used as a standard condition for the plots within this study.

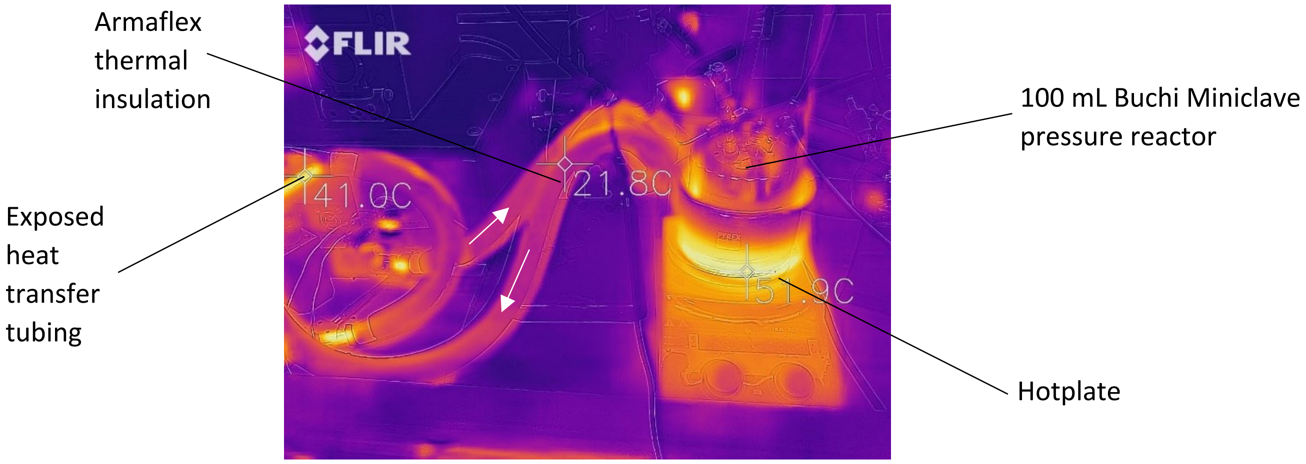

Figure S14: Thermal image of the FlowNMR setup (reactor to pump) during a flow run with the reaction vessel, flow path and flow tube heated to 50°C. Crosshairs indicate the surface temperature of the hotplate, Armaflex insulation and heat exchanger tubing.

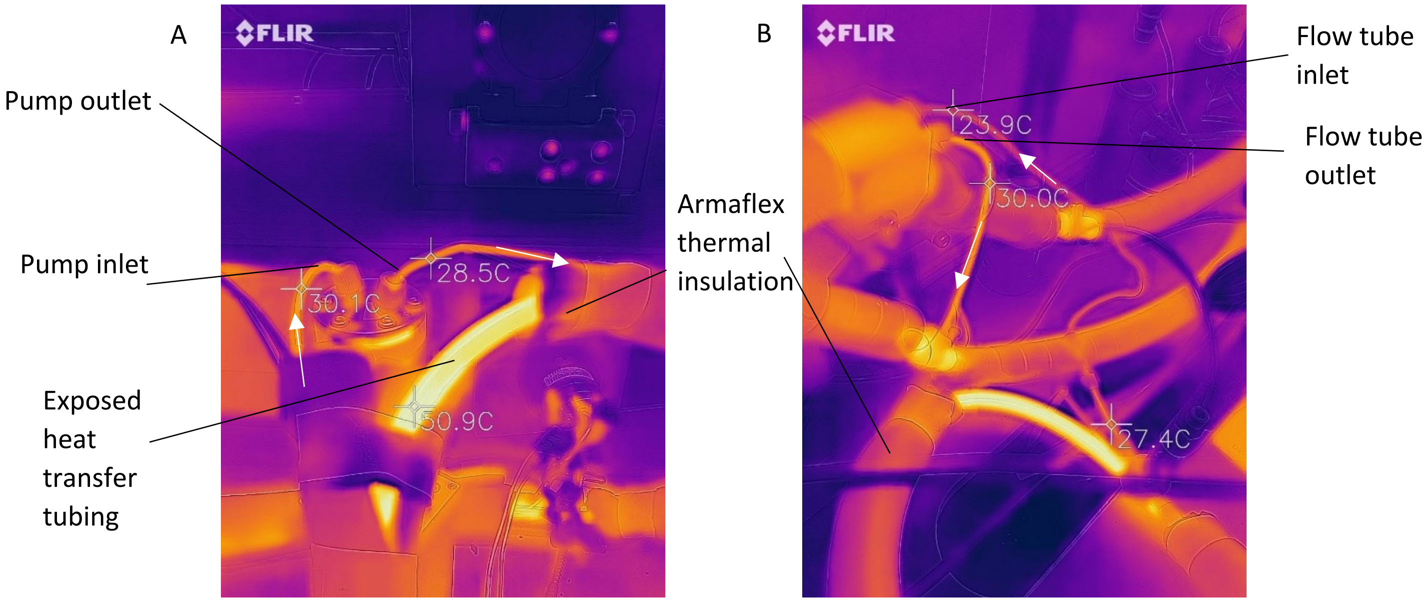

Figure S15: Thermal image of the FlowNMR setup at the inlet and outlet of the HNP-M Mzr-2921X1-hs-vb pump (A) and the interface between the flow path and the flow tube (B), during a flow run with the reaction vessel, flow path and flow tube heated to 50°C. Crosshairs indicate the surface temperature of the pump inlet, pump outlet and heat exchanger tubing (A) and the flow tube inlet, flow tube outlet (B).

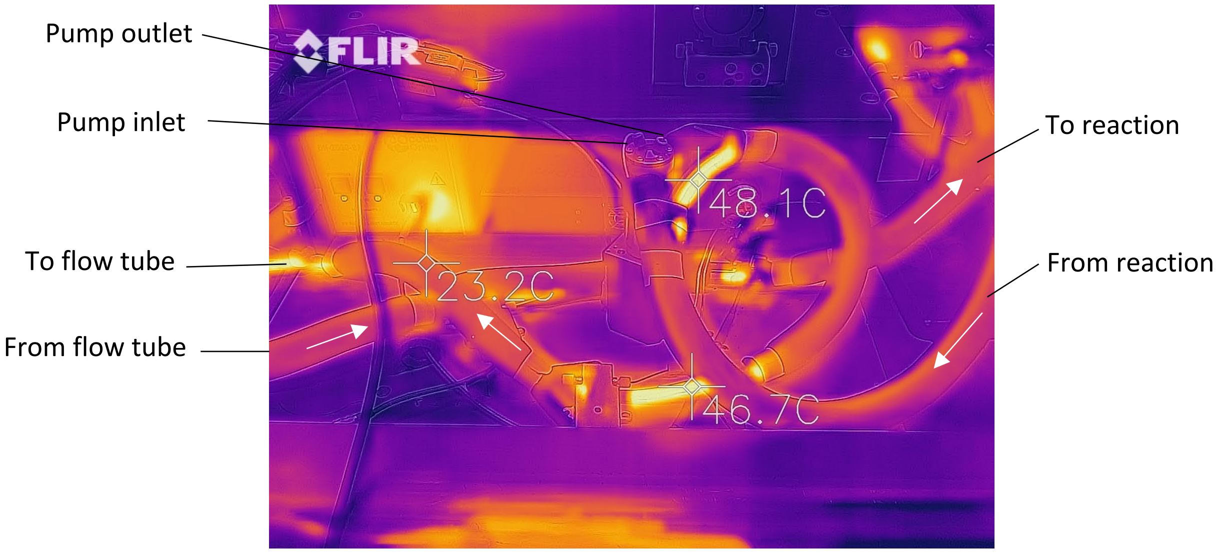

Figure S16: Thermal image of the FlowNMR setup at the inlet and outlet of the HNP-M Mzr-2921X1-hs-vb pump during a flow run with the reaction vessel, flow path and flow tube heated to 50°C. Crosshairs indicate the surface temperature of the heat exchanger tubing and Armaflex insulation.

10.0 Pumps

10.1 Residence Time Distribution

Residence time distribution can be utilised to characterise the behaviour of reactors and flow systems.[22-25] Step injection experiments were performed in this study to obtain the RTD profiles. A tracer (fluorescein) was injected into the reactor at t = 0 to determine the RTD experimentally by measuring the tracer's concentration, C, in the effluent stream as a function of time. The concentration at the outlet was measured by UV-vis spectroscopy at a constant flow rate (1-6 mL/min), until the concentration of tracer in the flow path to the reaction vessel was saturated in the effluent. The absorbance data was normalised to the concentration obtaining the non-dimensional curve F(t) going from 0 to 1.

$$F(t) = \frac{C(t)}{C_0}$$

Equation S14

The cumulative distribution F(t) can be determined directly from a step input. The variable C(t) is the concentration at time t. Creating this normalised distribution function allows flow performances of different magnitudes inside the system to be compared directly.

The step and pulse responses were then related by:

$$F(t) = \int_0^t E(t')dt'$$

Equation S15

$$E(t) = \frac{dF(t)}{dt}$$

Equation S16

Where E(t) is the RTD function of the setup.

The following plots show the residence time distributions of all the other positive displacement pumps discussed in this paper, at the 6 different flow rates used (1-6 mL/min):

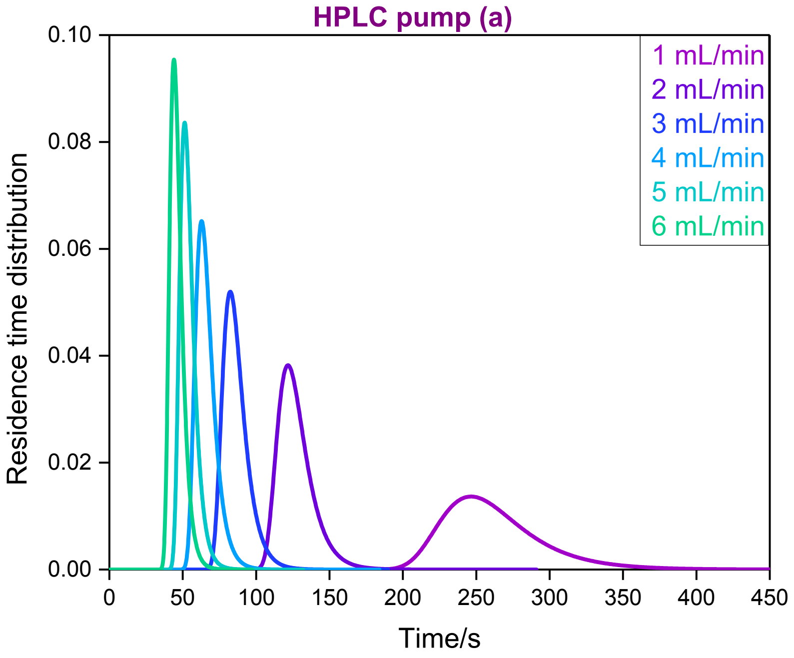

Figure S17. RTD profiles of the FlowNMR apparatus with HPLC pump as derived from FlowUV-vis spectroscopy at 334 nm using 12 mM fluorescein in acetone as the marker in a step change displacement experiment, at 1-6 mL/min at 25˚C.

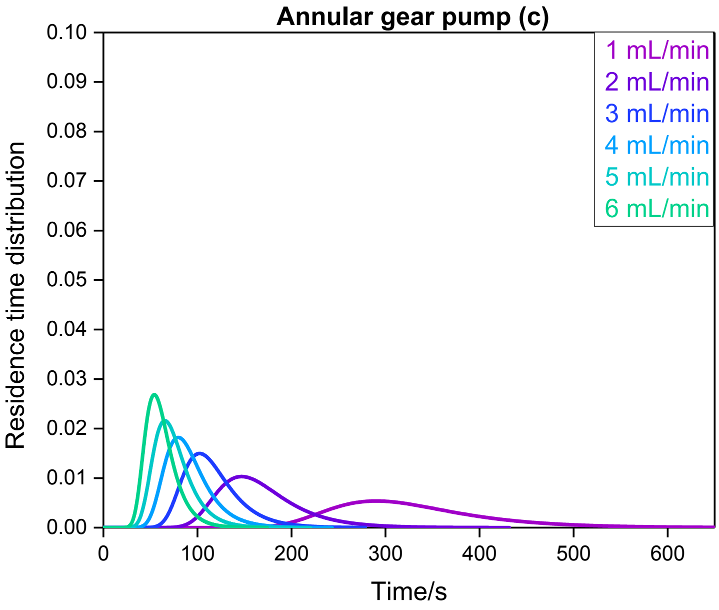

Figure S18. RTD profiles of the FlowNMR apparatus with Annular gear pump as derived from FlowUV-vis spectroscopy at 334 nm using 12 mM fluorescein in acetone as the marker in a step change displacement experiment, at 1-6 mL/min at 25˚C.

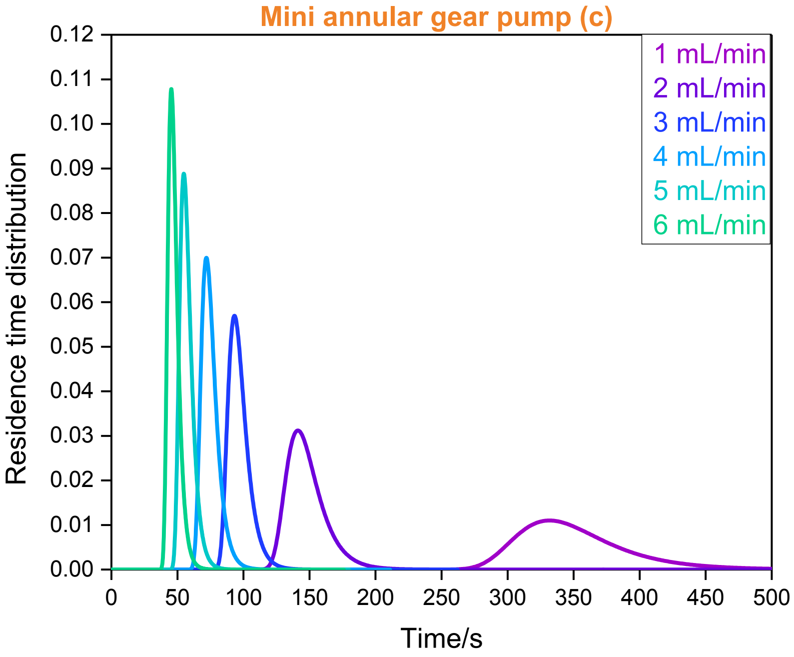

Figure S19. RTD profiles of the FlowNMR apparatus with Mini-Annular gear pump as derived from FlowUV-vis spectroscopy at 334 nm using 12 mM fluorescein in acetone as the marker in a step change displacement experiment, at 1-6 mL/min at 25˚C.

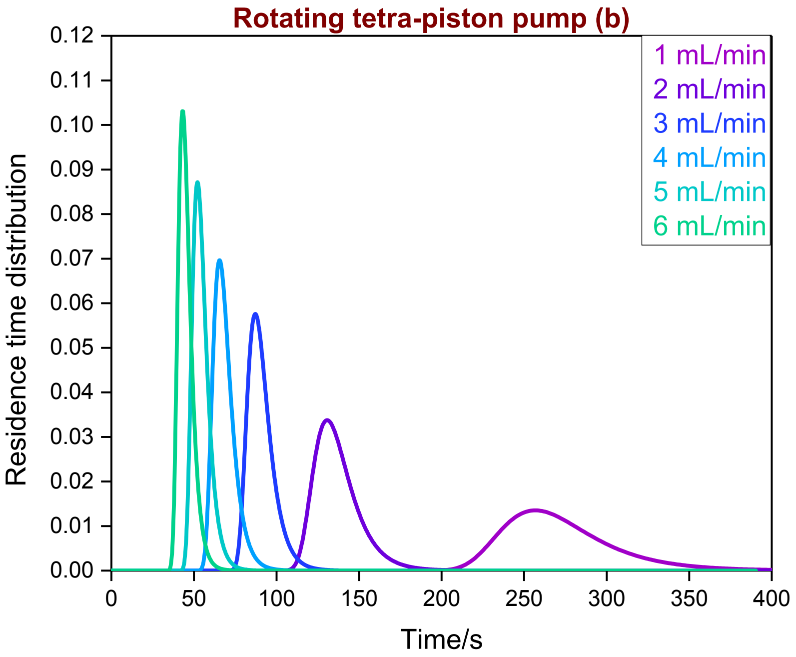

Figure S20. RTD profiles of the FlowNMR apparatus with Rotary tetra-piston pump as derived from FlowUV-vis spectroscopy at 334 nm using 12 mM fluorescein in acetone as the marker in a step change displacement experiment, at 1-6 mL/min at 25˚C.

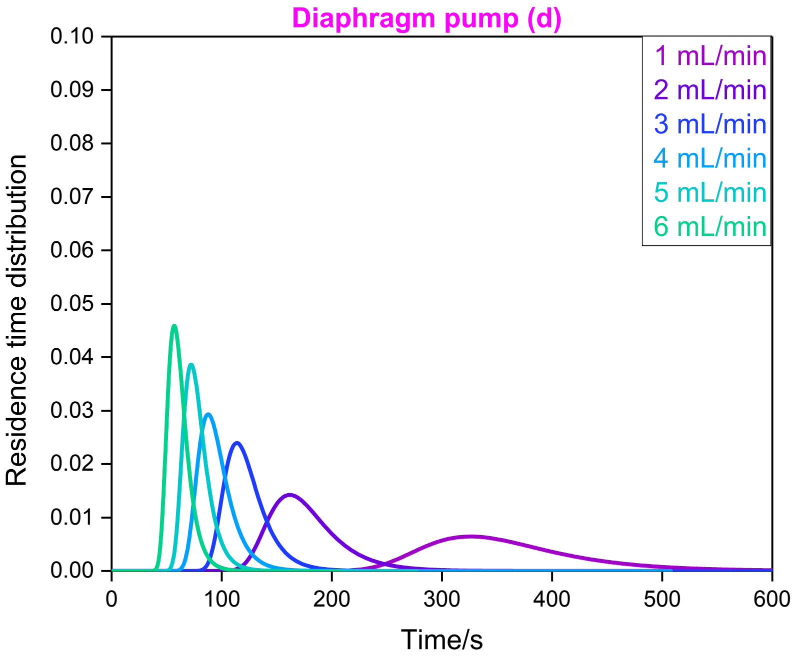

Figure S21. RTD profiles of the FlowNMR apparatus with Diaphragm pump as derived from FlowUV-vis spectroscopy at 334 nm using 12 mM fluorescein in acetone as the marker in a step change displacement experiment, at 1-6 mL/min at 25˚C.

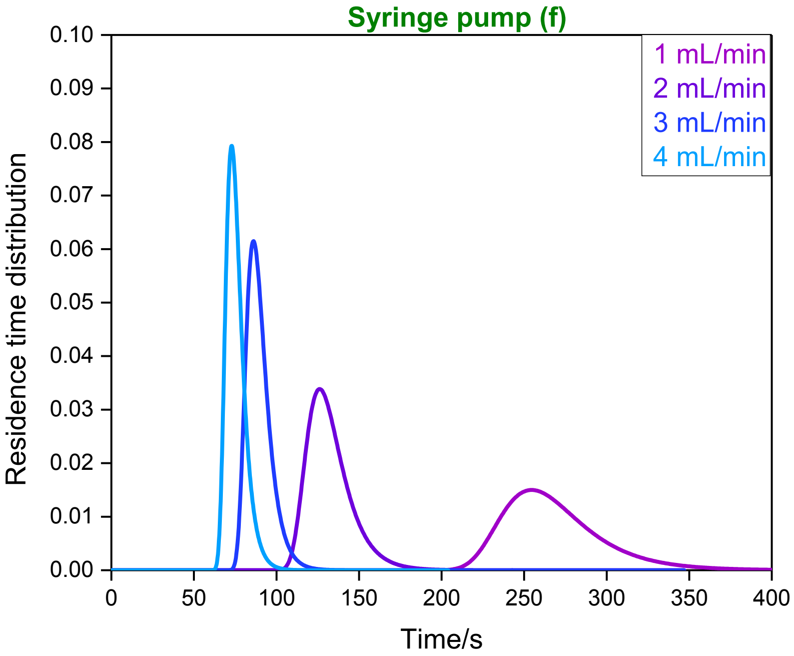

Figure S22. RTD profiles of the FlowNMR apparatus with Syringe pump as derived from FlowUV-vis spectroscopy at 334 nm using 12 mM fluorescein in acetone as the marker in a step change displacement experiment, at 1-4 mL/min at 25˚C.

The

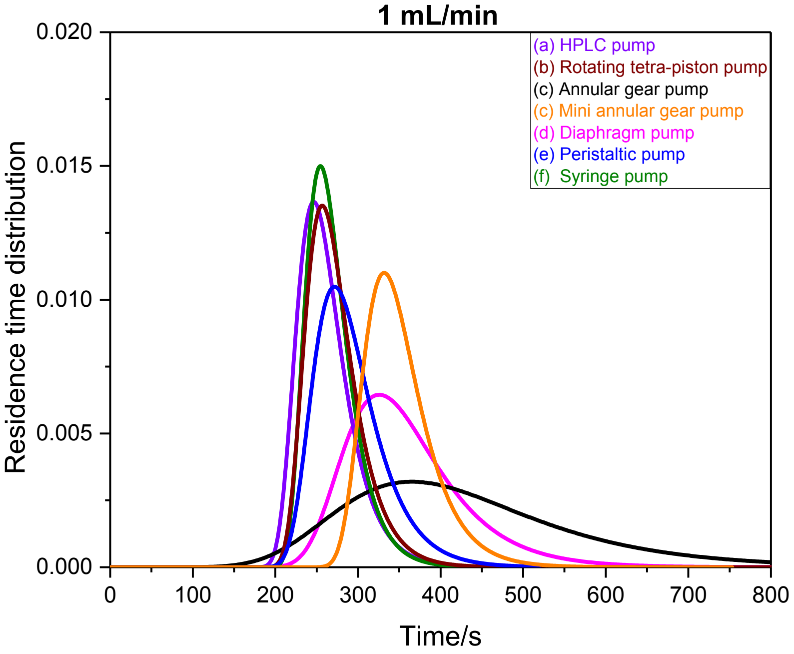

following plots show RTD overlays of all pumps at each specific flowrate tested:

Figure S23. Overlay of RTD profiles of the FlowNMR apparatus with all PD pumps as derived from FlowUV-vis spectroscopy at 334 nm using 12 mM fluorescein in acetone as the marker in a step change displacement experiment, at 1 mL/min at 25˚C.

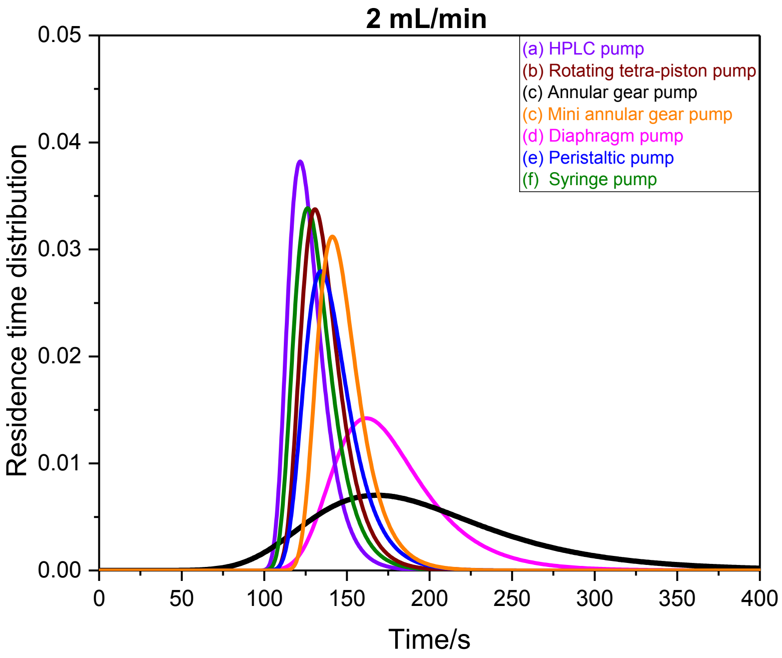

Figure S24. Overlay RTD profiles of the FlowNMR apparatus with all PD pumps as derived from FlowUV-vis spectroscopy at 334 nm using 12 mM fluorescein in acetone as the marker in a step change displacement experiment, at 2 mL/min at 25˚C.

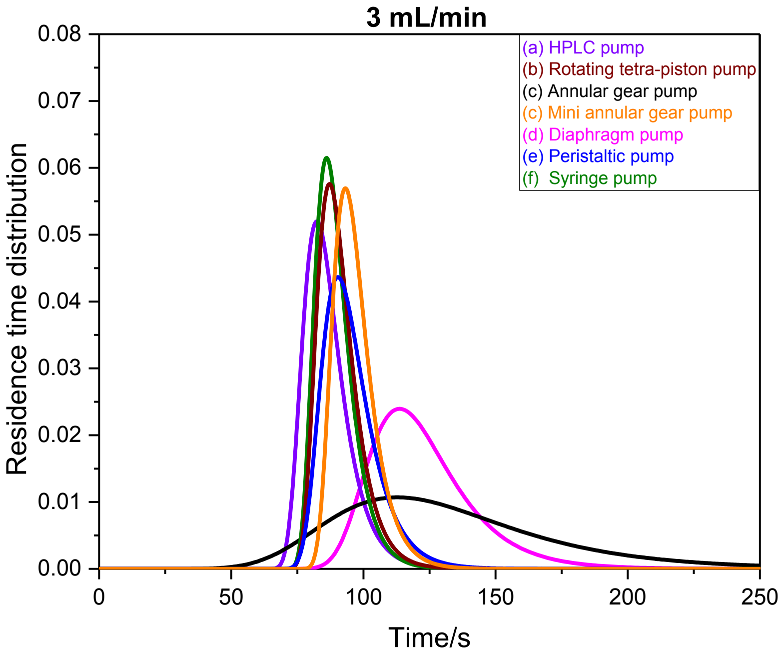

Figure S25. Overlay RTD profiles of the FlowNMR apparatus with all PD pumps as derived from FlowUV-vis spectroscopy at 334 nm using 12 mM fluorescein in acetone as the marker in a step change displacement experiment, at 3 mL/min at 25˚C.

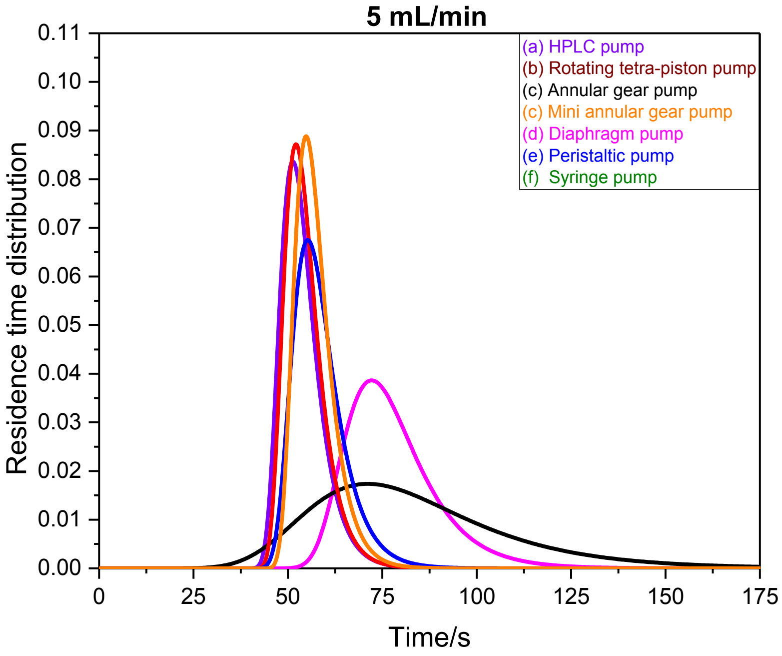

Figure S26. Overlay RTD profiles of the FlowNMR apparatus with all PD pumps as derived from FlowUV-vis spectroscopy at 334 nm using 12 mM fluorescein in acetone as the marker in a step change displacement experiment, at 5 mL/min at 25˚C.

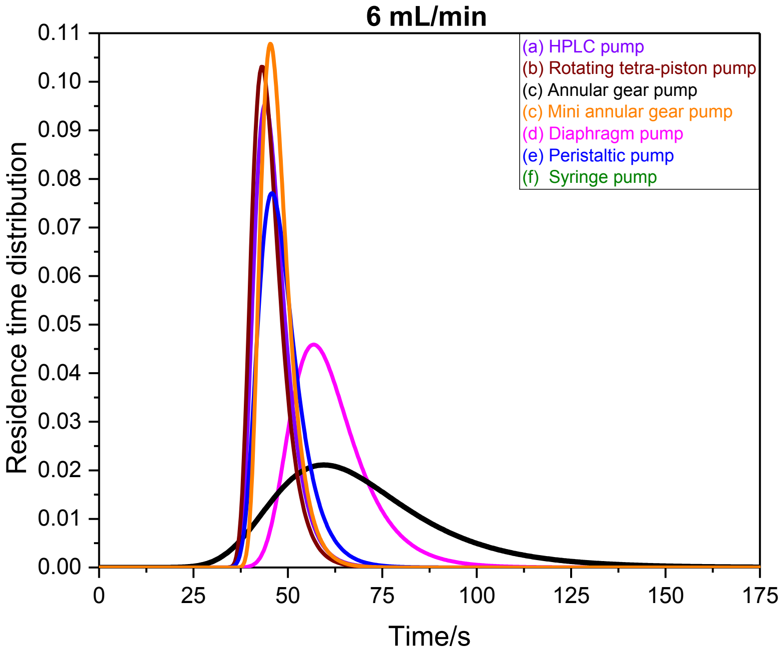

Figure S27. Overlay RTD profiles of the FlowNMR apparatus with all PD pumps as derived from FlowUV-vis spectroscopy at 334 nm using 12 mM fluorescein in acetone as the marker in a step change displacement experiment, at 6 mL/min at 25˚C.

10.1.1 Mean residence time (τ) for each experiment

Mathematical equation to calculate τ (mean hydrodynamic residence time):

$$\tau = \frac{\sum t_i C_i}{\sum C_i}$$

Equation S17

Where *ti* is Ith observation of time, where I represents the sample points, *Ci* is the residence time at the Ith observation of the tracer output, where I is the sample points.

or

$$\tau = \int_{o}^{\infty} tE(t)\ \mathrm{d}t$$

Equation S18

The mean value of the variable is equal to the first moment of the RTD function, E(t). The area under the curve of a plot of tE(t) as a function of t will yield τ.

Where τ is large, this shows a slow decay of the output transient, C(t), and E(t) for a pulse input. Where τ is small, this shows a rapid decay of the transient, C(t), and E(t) for a pulse input.

Table S8. Mean residence times calculated from the RTD profiles of the FlowNMR apparatus with all PD pumps as derived from FlowUV-vis spectroscopy at 334 nm using 12 mM fluorescein in acetone as the marker in a step change displacement experiment, at 1-6 mL/min at 25˚C.

	τ / seconds					
Pump	1 mL/min	2 mL/min	3 mL/min	4 mL/min	5 mL/min	6 mL/min
Peristaltic	291.9 ± 15.6	141.7 ± 8.1	95 ± 5.8	72.8 ± 4.7	58.3 ± 4.0	48.4 ± 3.4
HPLC	261.8 ± 13.7	127.1 ± 7.4	86.4 ± 2.8	66.1 ± 3.1	53.8 ± 3.7	46.2 ± 2.9
Diaphragm	358.3 ± 8.2	176.6 ± 4.5	122.5 ± 3.4	94.9 ± 2.2	77.7 ± 2.6	61.4 ± 2.2
Annular Gear	430.9 ± 6.2	197.8 ± 5.0	132.2 ± 3.7	103.3 ± 2.5	83.2 ± 2.5	69.5 ± 1.8
Mini annular gear	350.6 ± 8.0	148.0 ± 4.5	96.9 ± 3.0	75.0 ± 1.7	57.2 ± 1.8	47.3 ± 1.6
Rotary tetra-piston	272.1± 14.6	136.9 ± 7.8	90.8 ± 5.6	68.5 ± 4.1	54.6 ± 3.7	45.2 ± 3.7
Syringe	268.3 ± 5.0	132.3 ± 3.7	89.5 ± 2.3	75.5 ± 2.5	-	-

Total volume of flowpath with corresponding pump using experimental τ calculated:

Table S9. Internal pump volume calculated from the RTD profiles of the FlowNMR apparatus with all PD pumps as derived from FlowUV-vis spectroscopy at 334 nm using 12 mM fluorescein in acetone as the marker in a step change displacement experiment, at 1-6 mL/min at 25˚C.

	Volume / mL					
Pump	1 mL/min	2 mL/min	3 mL/min	4 mL/min	5 mL/min	6 mL/min
Peristaltic	4.85 ± 0.06	4.72 ± 0.07	4.75 ± 0.06	4.85 ± 0.03	4.86 ± 0.02	4.84 ± 0.02
HPLC	4.76 ± 0.07	4.74 ± 0.05	4.79 ± 0.04	4.74 ± 0.03	4.78 ± 0.03	4.72 ± 0.04
Diaphragm	5.97 ± 0.05	5.89 ± 0.04	6.13 ± 0.02	6.32 ± 0.06	6.47 ± 0.03	6.14 ± 0.02
Annular Gear	6.46 ± 0.07	6.56 ± 0.03	6.79 ± 0.04	6.76 ± 0.05	6.23 ± 0.07	7.18 ± 0.04
Mini annular gear	5.84 ± 0.09	4.73 ± 0.02	4.85 ± 0.04	4.80 ± 0.01	4.77 ± 0.03	4.75 ± 0.02
Rotary tetra-piston	4.53 ± 0.03	4.57 ± 0.02	4.54 ± 0.03	4.57 ± 0.02	4.55 ± 0.02	4.52 ± 0.05
Syringe	4.47 ± 0.07	4.41 ± 0.01	4.43 ± 0.02	4.43 ± 0.02	-	-

10.1.2 Propagation of uncertainty:

A propagation of uncertainty analysis was carried out to ascertain the effect of the individual variables' deviation on the uncertainty of our results from our residence time distribution (RTD) experiments. The approach of combining individual experimental uncertainties on the input parameters to obtain the deviation on the output is not applicable in this case, because there is no single equation linking the input parameters to the output (intermediate fitting step). Our approach was therefore to estimate the experimental deviation of the variables demonstrating the highest magnitude of deviation (namely the flow rate and absorbance) to propagate their effects on the final parameters calculated. They were set to their maximal deviations (nominal value of 5% and 3.5% respectively) at a representative value, after which the fitting process was applied, and the output parameters were then compared to what they came out to be with the nominal value of the input. This difference on the output was then used as an estimate of its uncertainty to calculate the deviation associated with the mean residence time (τ). This method resembles a Monte-Carlo simulation of uncertainty propagation,[26] i.e. varying the input together, within the limits of their distribution and watching how much the output varies.

The RTD data obtained was then fitted to the CSTR cascade model where the method used to fit the data was to minimise the sum of absolute values of differences between the observed data and the CSTR cascade by changing the parameters. We found a curve of best fit by using a series of solutions from the Broyden–Fletcher–Goldfarb–Shanno algorithm (BFGS)[27] and a form of a random walk to explore the surfaces, using the textbook equations as an initial starting point. A new starting point very close to the best solution was then picked and the BFGS was run again to obtain the new solution. This was repeated until the best solution wasn't modified for a fixed number of steps. This heuristic allowed for the exploration of the surface by retaining the best solution while testing many alternative sensible starting points, thus giving confidence about the quality of the obtained solution when the algorithm converged to one best solution. This stochastic method (BFGS) was run from several starting points then recorded and analysed the obtained solutions. This was repeated five times to generate an average for the output parameters (vessel and tailing numbers etc).

10.1.3 Fitting the RTD to a cascade of ideal CSTRs:

The hydrodynamics dictate whether the RTD of a real reactor deviates from that of an ideal reactor. A variance greater than 0 suggests dispersion in the apparatus which could be due to turbulence, diffusion, or a non-uniform velocity profile. An ideal CSTR is characterised by the instantaneous and complete mixing of the flow at the inlet of the apparatus, as well as the same homogenous composition during all times in the apparatus.

The RTD is an exponential which can be written as:

$$E(\tau) = \frac{1}{T}e\frac{-\tau}{T}$$

Equation S19

In this type of reactor, the mean is T and variance is 1, and the fluid placed into the system is never completely gone. Obtaining mixing instantaneously is not feasible due to the delay between any fluid passing from the inlet to the outlet. The RTD of a real reactor therefore deviates from the desired exponential decay. E will be subject to a finite delay before reaching its maximum or minimum value, which will be indicative of the rate of mass transfer in the reactor.

The CSTR cascade equation used to model RTD corresponds to:

$$\tau E(t) = \left(\frac{t}{\tau}\right)^{N-1}\frac{N^N}{(N-1)!}e^{-\frac{tN}{\tau}}$$

Equation S20

Generalizing this method to a series of *n* CSTRs gives the RTD for *n* CSTRs in series, E(t).

We analysed the residence time distribution to determine the number of ideal vessels, *n*, in series that give around the same residence time distribution as the nonideal flow system investigated. As *n* gets larger, the characteristics of the flow setup approach those of an ideal plug flow reactor.

Mathematical equation to calculate the variance of the residence time:

$$\sigma^2 = \frac{\sum t_i^2 C_i}{\sum C_i} - \tau^2$$

Equation S21

Mathematical equation used to calculate an approximation of *N (tanks in series)* to allow for a starting point for fitting the RTD data with the CSTR model:

$$N = \frac{\tau^2}{\sigma^2} = \frac{\left(\frac{\sum t_i C_i}{\sum C_i}\right)^2}{\frac{\sum t_i^2 C_i}{\sum C_i} - \tau^2}$$

Equation S22

The following plots show the best fit of RTD together with the best CSTR model we were able to find using the method described above. The following graphs show the fitting of the CSTR model to the data:

HPLC pump (a)

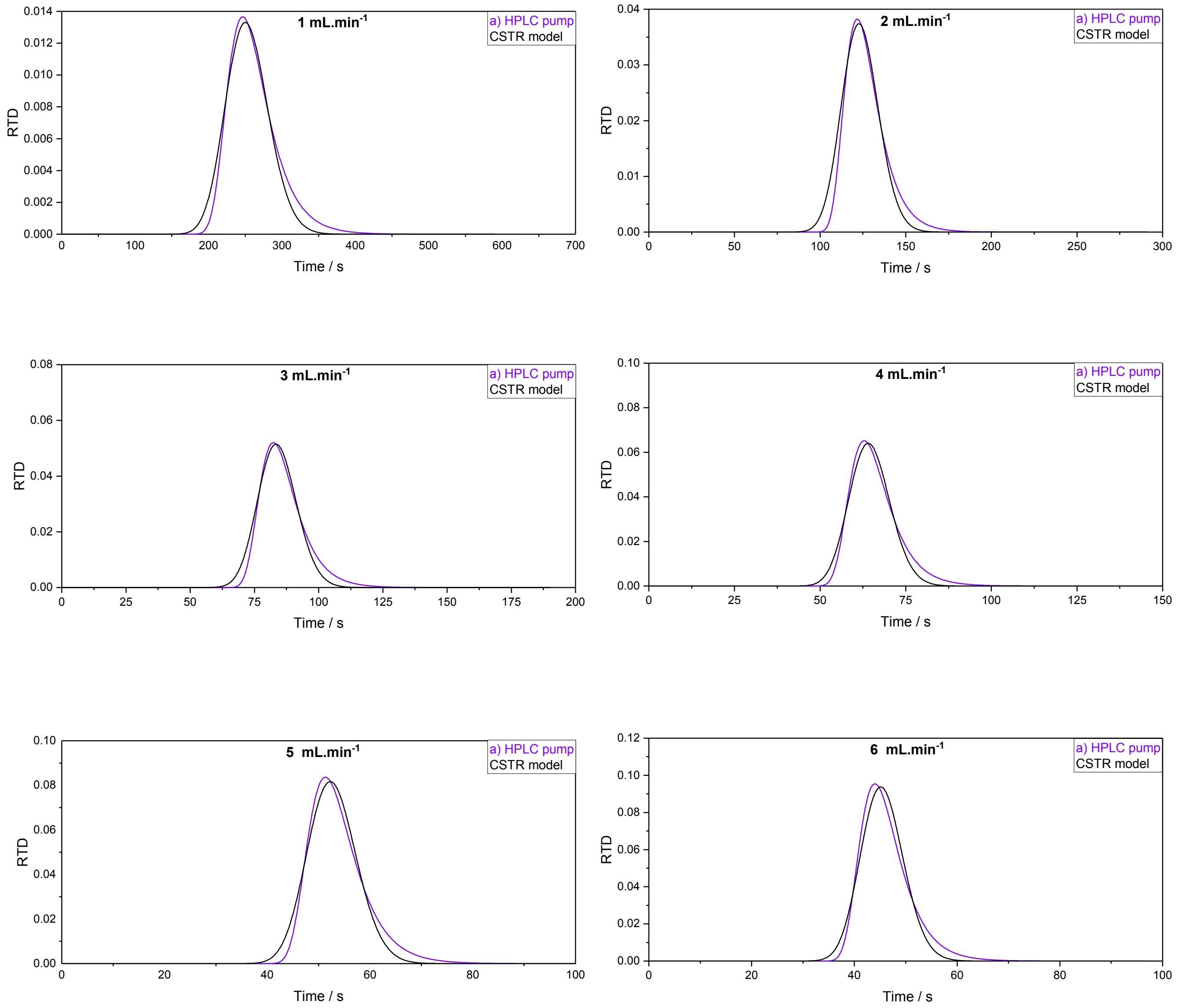

Figure S30. RTD profiles of the FlowNMR apparatus fitted to CSTR model for the double-piston HPLC pump as derived from FlowUV-vis spectroscopy at 334 nm using 12 mM fluorescein in acetone as the marker in a step change displacement experiment, at 1-6 mL/min at 25˚C.

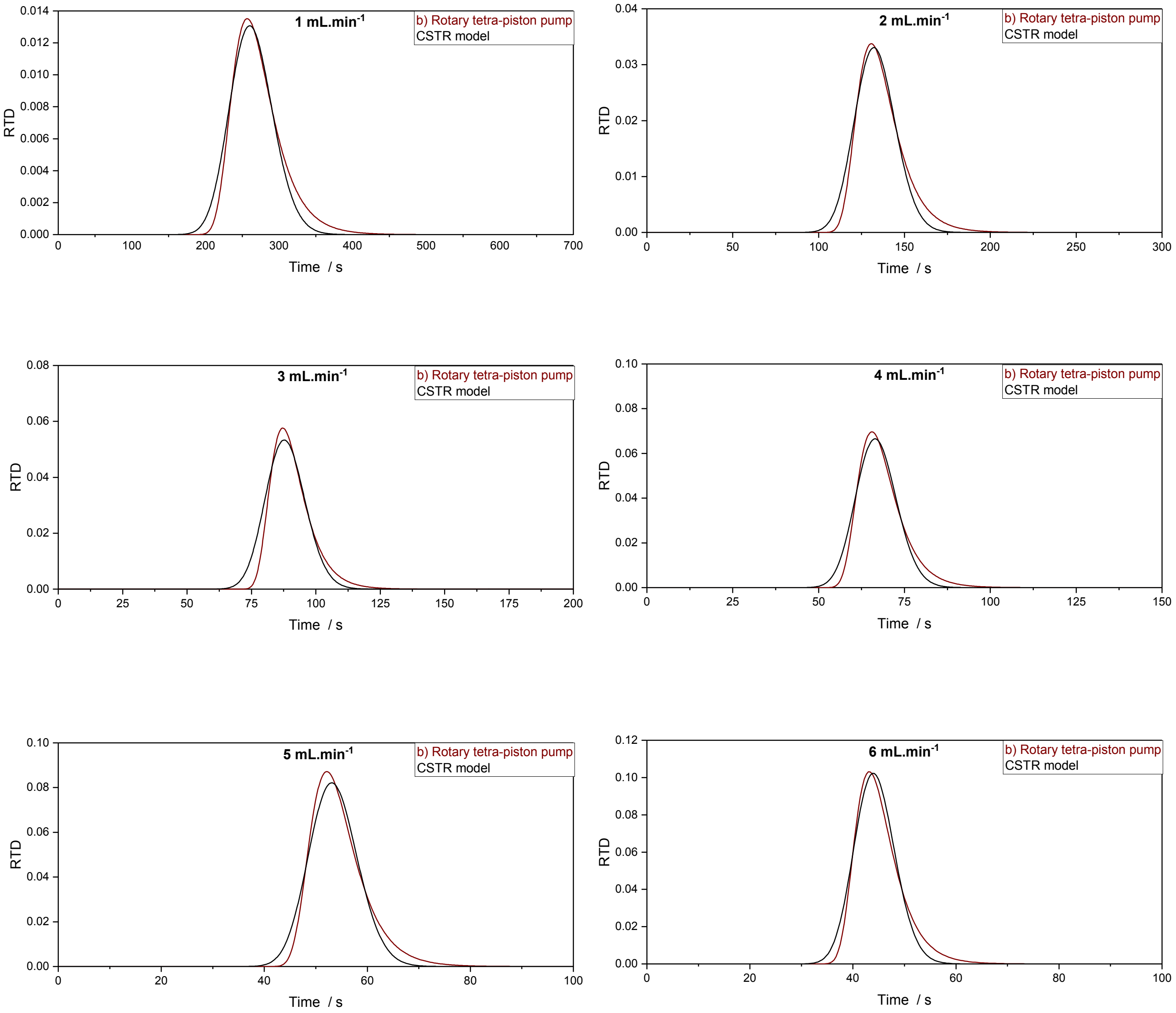

Rotary tetra-piston pump (b)

Figure S34. RTD profiles of the FlowNMR apparatus fitted to CSTR model for the rotary tetra-piston pump as derived from FlowUV-vis spectroscopy at 334 nm using 12 mM fluorescein in acetone as the marker in a step change displacement experiment, at 1-6 mL/min at 25˚C.

Annular Gear pump (c)

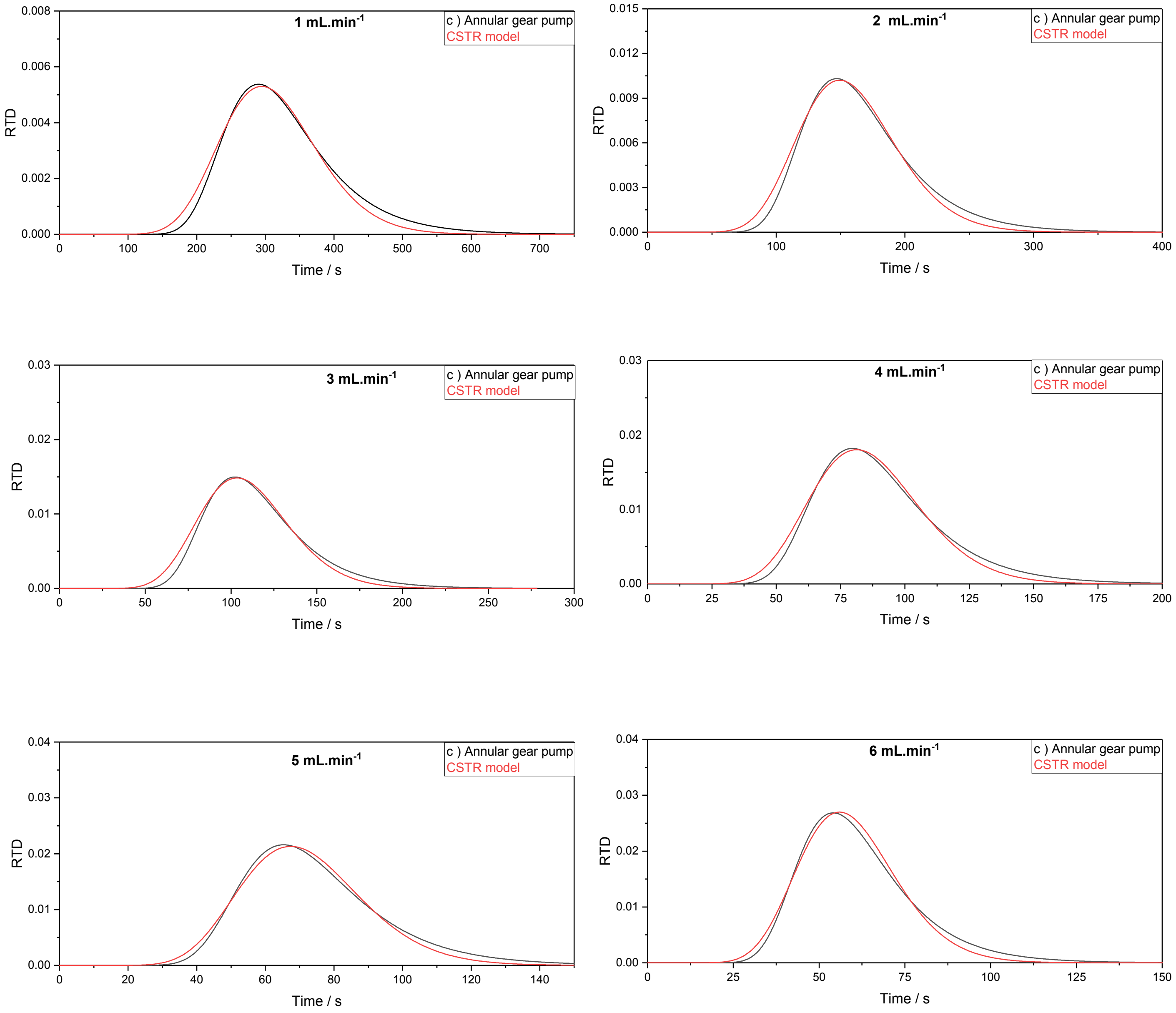

Figure S29. RTD profiles of the FlowNMR apparatus fitted to CSTR model for the annular gear pump as derived from FlowUV-vis spectroscopy at 334 nm using 12 mM fluorescein in acetone as the marker in a step change displacement experiment, at 1-6 mL/min at 25˚C.

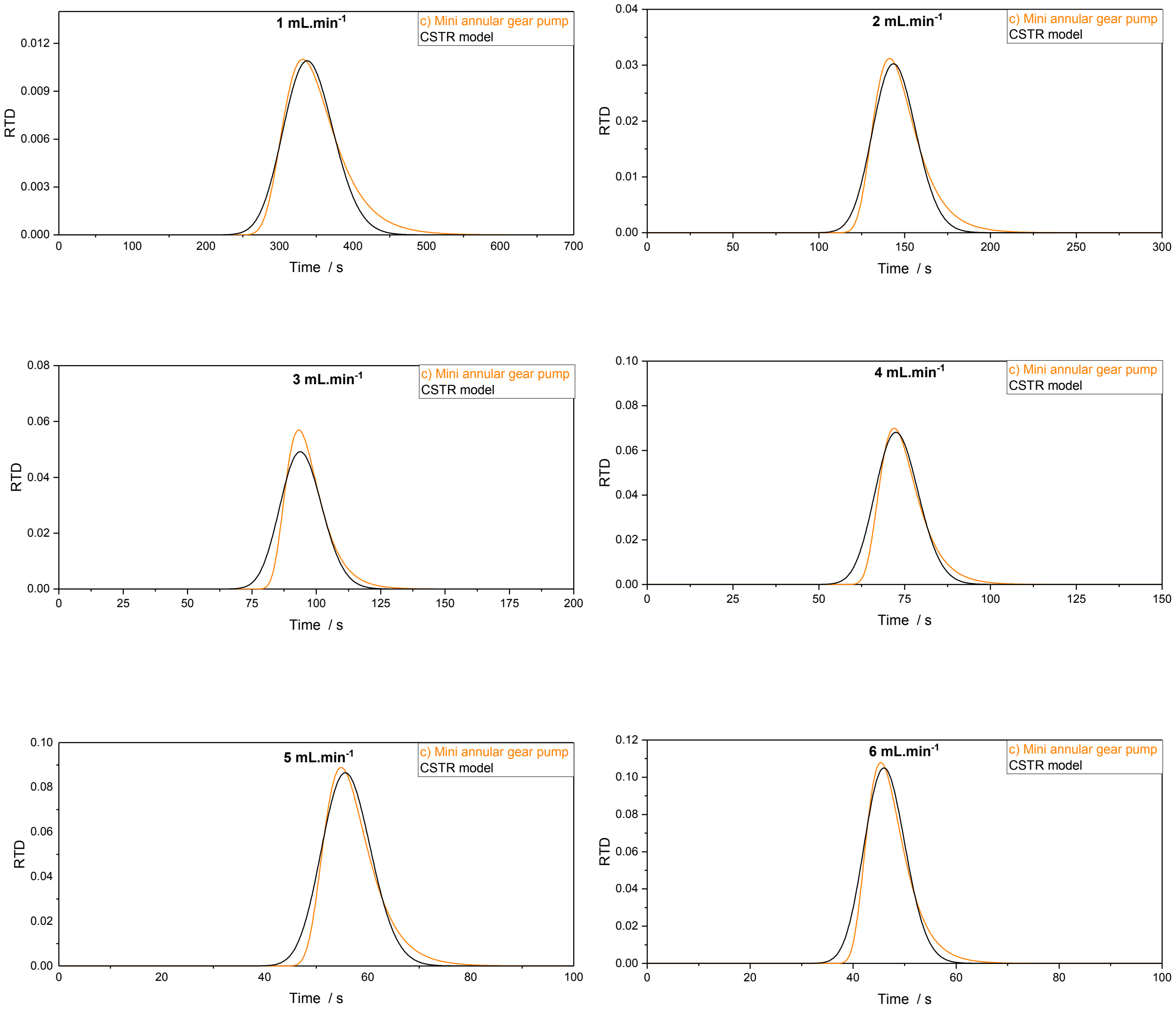

Mini annular gear pump (c)

Figure S28. RTD profiles of the FlowNMR apparatus fitted to CSTR model for the mini annular gear pump as derived from FlowUV-vis spectroscopy at 334 nm using 12 mM fluorescein in acetone as the marker in a step change displacement experiment, at 1-6 mL/min at 25˚C.

Diaphragm pump (d)

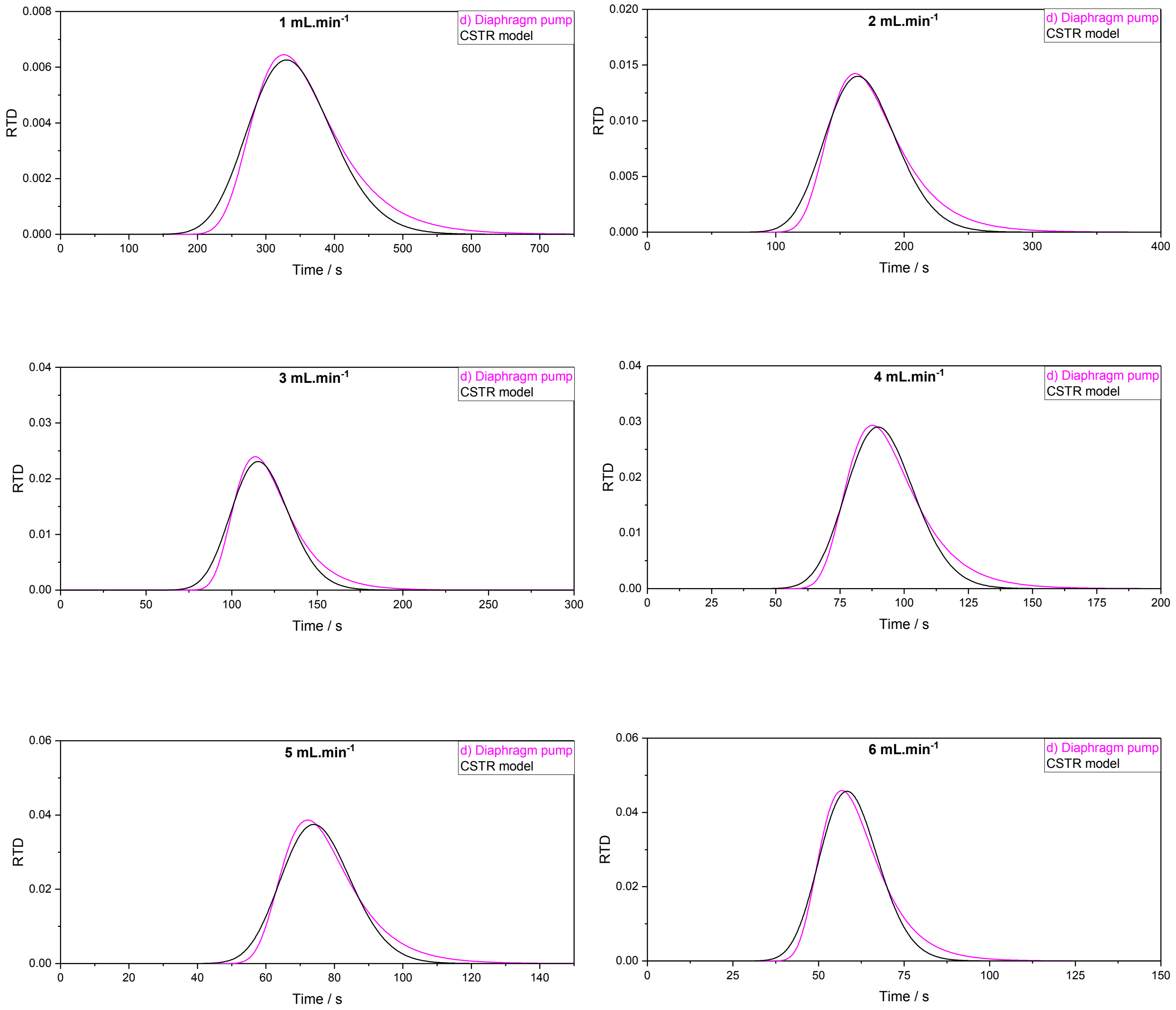

Figure S32. RTD profiles of the FlowNMR apparatus fitted to CSTR model for the diaphragm pump as derived from FlowUV-vis spectroscopy at 334 nm using 12 mM fluorescein in acetone as the marker in a step change displacement experiment, at 1-6 mL/min at 25˚C.

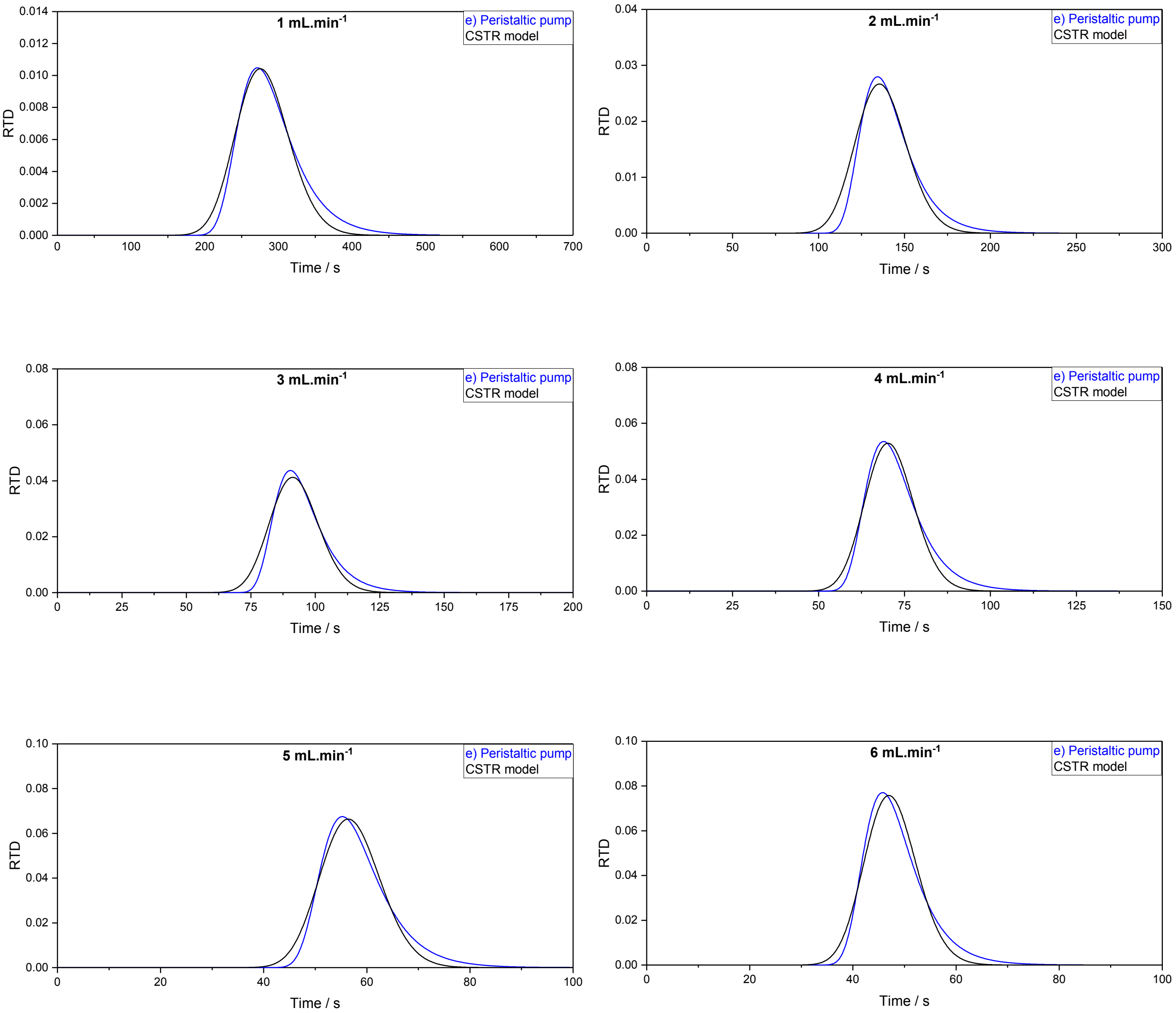

Peristaltic pump (e)

Figure S33. RTD profiles of the FlowNMR apparatus fitted to CSTR model for the peristaltic pump as derived from FlowUV-vis spectroscopy at 334 nm using 12 mM fluorescein in acetone as the marker in a step change displacement experiment, at 1-6 mL/min at 25˚C.

Syringe pump (f)

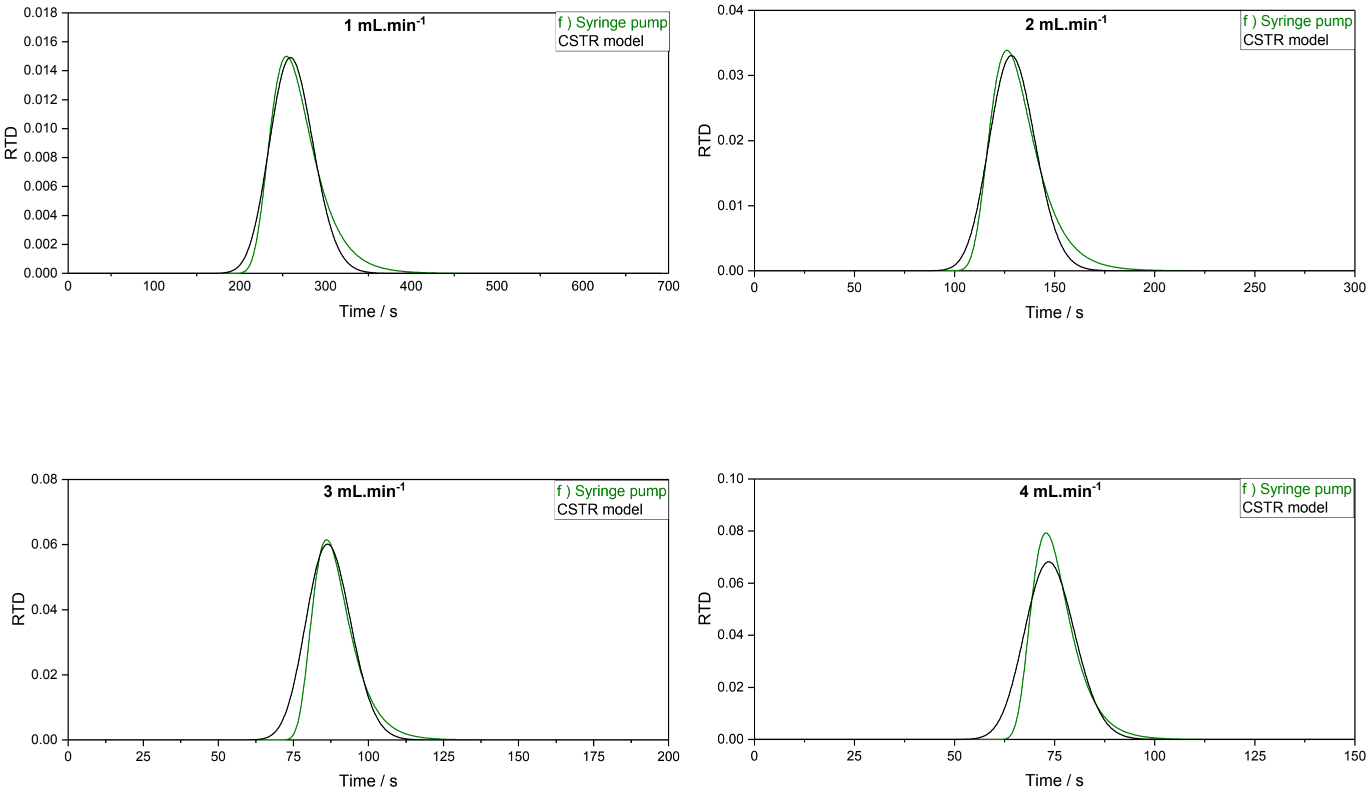

Figure S31. RTD profiles of the FlowNMR apparatus fitted to CSTR model for the syringe pump as derived from FlowUV-vis spectroscopy at 334 nm using 12 mM fluorescein in acetone as the marker in a step change displacement experiment, at 1-4 mL/min at 25˚C.

Table S10. CSTR cascade vessel numbers for the FlowNMR setup shown as derived from Gaussian fits of their RTD profiles.

	Vessel number / N					
Pump	1 mL/min	2 mL/min	3 mL/min	4 mL/min	5 mL/min	6 mL/min
Peristaltic	60 ± 5	102 ± 4	106 ± 5	102 ± 2	104 ± 5	89 ± 4
Double-piston HPLC	77 ± 3	133 ± 2	129 ± 3	118 ± 6	126 ± 7	119 ± 4
Diaphragm	31 ± 2	37 ± 5	49 ± 4	45 ± 3	51 ± 3	45 ± 4
Annular Gear	16 ± 2	15 ± 2	16 ± 2	14 ± 1	14 ± 2	15 ± 1
Mini annular gear	101 ± 3	132 ± 3	135 ± 2	133 ± 2	135 ± 4	136 ± 2
Rotary tetra-piston	82 ± 2	128 ± 2	132 ± 3	129 ± 2	130 ± 2	128 ± 3
Syringe	104 ± 3	125 ± 3	136 ± 4	136 ± 4	--	--

Table S11. Bodenstein number calculated from the vessel number as derived from Gaussian fits of their RTD profiles.

	Bodenstein / B_o					
Pump	1 mL/min	2 mL/min	3 mL/min	4 mL/min	5 mL/min	6 mL/min
Peristaltic	120 ± 10	204 ± 8	212 ± 10	204 ± 4	208 ± 10	178 ± 8
Double-piston HPLC	154 ± 6	266 ± 4	258 ± 6	236 ± 12	252 ± 14	238 ± 8
Diaphragm	62 ± 4	74 ± 10	98 ± 8	90 ± 6	102 ± 6	90 ± 8
Annular Gear	32 ± 4	30 ± 4	32 ± 4	28 ± 2	28 ± 4	30 ± 2
Mini annular gear	202 ± 6	264 ± 6	270 ± 4	266 ± 4	270 ± 8	272 ± 4
Rotary tetra-piston	164 ± 4	256 ± 4	264 ± 6	258 ± 4	260 ± 4	256 ± 6
Syringe	208 ± 6	250 ± 6	272 ± 8	272 ± 8	--	--

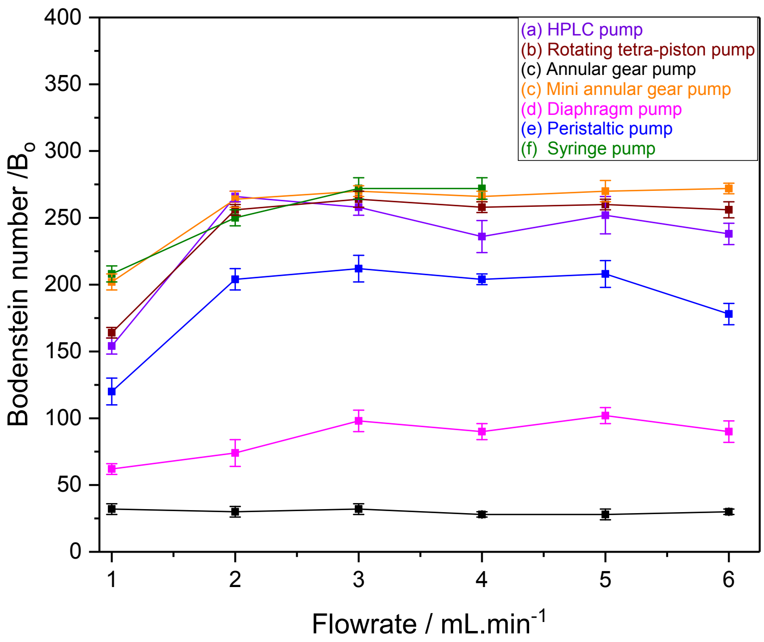

Figure S35: CSTR cascade Bodenstein numbers for the FlowNMR setup with all PD pumps as derived from Gaussian fits of their RTD profiles.

Equation used to calculate the area between the observed and the CSTR model curves.

$$I(d) = \int_{-\infty}^{\infty} E(t) - C(t)\,\mathrm{d}t$$

Equation S23

Table S12. Sample tailing from surface area differences.

	Tailing / %					
Pump	1mL/min	2 mL/min	3 mL/min	4 mL/min	5 mL/min	6 mL/min
Peristaltic	5.5 ± 0.3	7.0 ± 0.8	6.7 ± 0.3	7.7 ± 0.6	7.2 ± 0.5	6.3 ± 0.3
Double piston	6.6 ± 0.2	5.2 ±0.3	7.0 ± 0.2	6.8 ±0.3	6.8 ± 0.5	6.1 ± 1.0
Gear	4.4 ± 0.1	4.2 ± 0.5	4.4 ± 0.2	4.1 ± 0.1	4.0 ± 0.2	4.2 ± 0.2
Mini gear	4.7 ± 0.3	7.1 ± 0.4	4.4 ± 0.4	3.5 ± 0.3	4.7 ± 0.2	4.5 ± 0.3
Rotating tetra-piston	6.1 ± 0.5	6.3 ± 0.4	3.4 ± 0.3	5.7 ± 0.3	5.8 ± 0.3	6.6 ± 0.4
Diaphragm	5.2 ±0.3	6.0 ± 0.3	6.3 ± 0.2	5.8 ± 0.2	5.6 ± 0.2	5.5 ± 0.3
Syringe	6.6 ± 0.3	6.0 ± 0.3	3.0 ± 0.3	1.9 ± 0.3	--	--

10.2 RTD to flow tip

The following plots show the best fit of RTD together with the best CSTR model we were able to find using the methods described in 10.1.

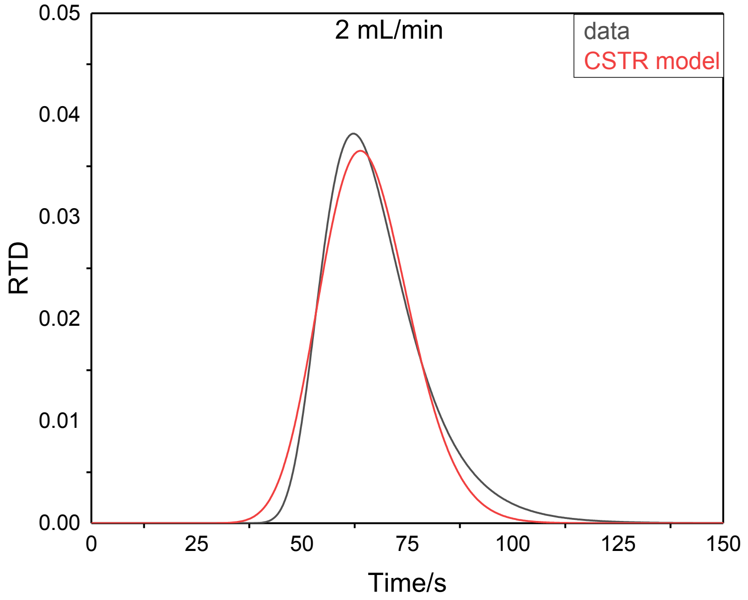

Figure S36. RTD profiles fitted to CSTR model for sample travel from the reaction vessel to the tip of the InsightMR™ flow tube using peristaltic pump (e) as derived from fast pulse ^{1}H NMR spectroscopic measurements using hexane to acetone in a step change displacement experiment at 2 mL/min.

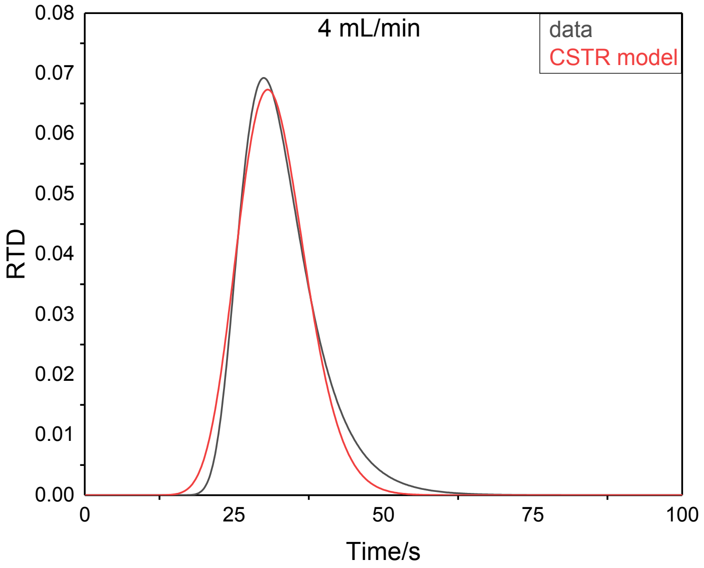

Figure S37. RTD profiles fitted to CSTR model for sample travel from the reaction vessel to the tip of the InsightMR™ flow tube using peristaltic pump (e) as derived from fast pulse ^{1}H NMR spectroscopic measurements using hexane to acetone in a step change displacement experiment at 4 mL/min.

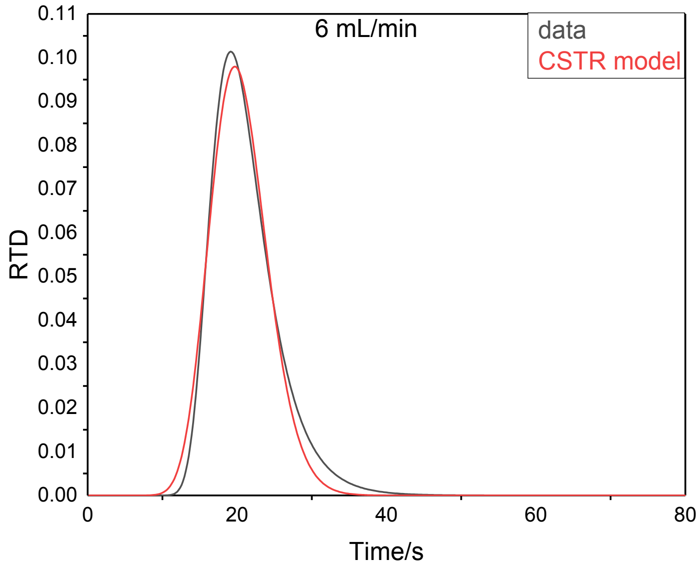

Figure S38. RTD profiles fitted to CSTR model for sample travel from the reaction vessel to the tip of the InsightMR™ flow tube using peristaltic pump (e) as derived from fast pulse ^{1}H NMR spectroscopic measurements using hexane to acetone in a step change displacement experiment at 6 mL/min

Table S13. Mean residence times, vessel numbers, Bodenstein numbers and degree of tailing calculated at three different flow rates RTD profiles for sample travel from the reaction vessel to the tip of the InsightMR™ flow tube using peristaltic pump as derived from fast pulse ^{1}H NMR spectroscopic measurements using hexane to acetone in a step change displacement experiment

	RTD to flowtube tip		
Flow rate	2 mL/min	4 mL/min	6 mL/min
τ / s	65.6 ± 4.0	31.7 ± 3.1	20.4 ± 2.6
n of ideal CSTRs	37 ± 4	31 ± 3	30 ± 4
Bodenstein number (B_o)	74 ± 8	62± 6	60± 8
Tailing / %	5.1 ± 0.6	5.4 ± 0.4	5.2 ± 0.3

10.3 Pump pulsation

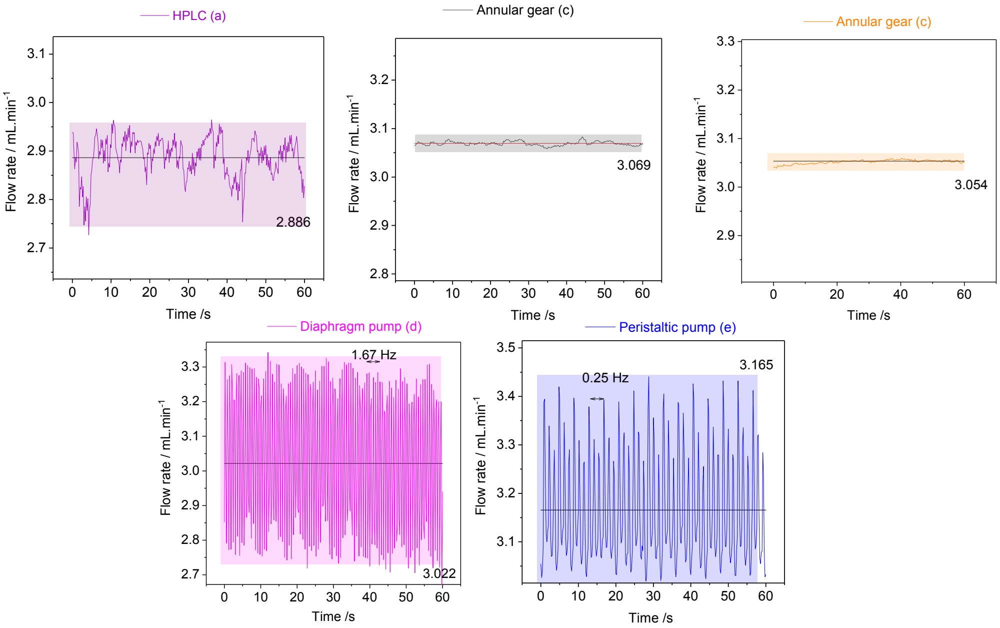

Figure S39. Flow rate oscillations due to pump pulsation as measured with a Bronkhorst mini Cori-Flow M13 for pumps (a-e) at a nominal flow rate of 3 mL/min acetone circulated through 1/16” PEEK tubing at room temperature. Black lines indicate the average flow rates delivered after external calibration.

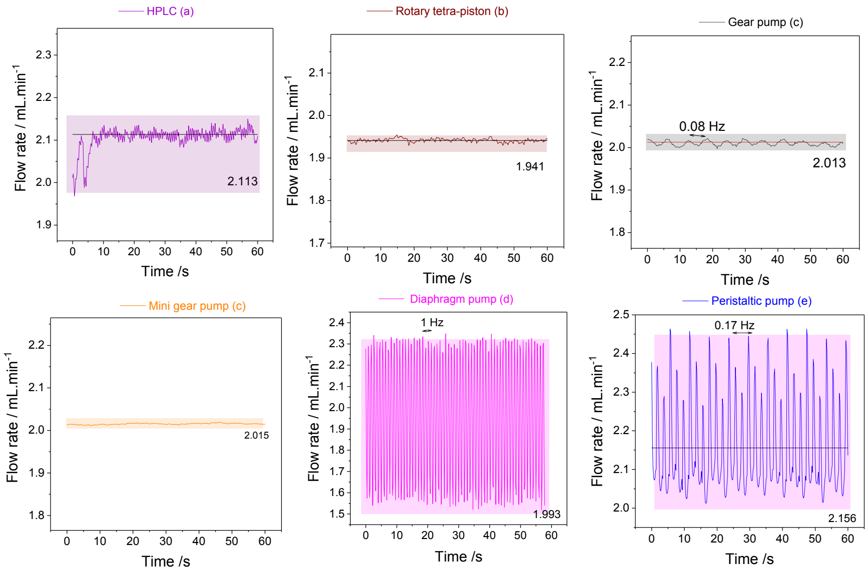

Figure S40. Flow rate oscillations due to pump pulsation as measured with a Bronkhorst mini Cori-Flow M13 for pumps (a-e) at a nominal flow rate of 2 mL/min acetone circulated through 1/16” PEEK tubing at room temperature. Black lines indicate the average flow rates delivered after external calibration.

Table S14. Flow rate and pulsation characterisation monitored using a Coriolis mass flow meter for the peristaltic pump at 2, 3 and 4 mL/min flowing toluene through 1/16” PEEK tubing at 25 °C under open-air atmospheric pressure.

Peristaltic pump (e)						
Flow rate / mL.min^{-1}	Mean / mL.min^{-1}	Maximum / mL.min^{-1}	Minimum / mL.min^{-1}	Minimum / %	Maximum / %	Frequency / Hz
4.00	4.18	4.56	3.96	-1.04	14.08	0.33
3.00	3.17	3.53	3.00	-0.03	17.57	0.25
2.00	2.16	2.49	1.96	-1.90	24.40	0.17

Table S15. Flow rate and pulsation characterisation monitored using a Coriolis mass flow meter for the diaphragm pump at 2, 3 and 4 mL/min flowing toluene through 1/16” PEEK tubing at 25 °C under open-air atmospheric pressure.

Diaphragm pump (d)						
Flow rate / mL.min^{-1}	Mean / mL.min^{-1}	Maximum / mL.min^{-1}	Minimum / mL.min^{-1}	Minimum / %	Maximum / %	Frequency / Hz
4.00	3.99	4.28	3.65	-8.72	7.08	2.50
3.00	3.02	3.34	2.64	-12.00	11.40	1.67
2.00	1.99	2.48	1.50	-24.90	24.10	1.00

Table S16. Flow rate and pulsation characterisation monitored using a Coriolis mass flow meter for the HPLC pump at 2, 3 and 4 mL/min flowing toluene through 1/16” PEEK tubing at 25 °C under open-air atmospheric pressure.

HPLC pump (a)					
Flow rate / mL.min^{-1}	Mean / mL.min^{-1}	Maximum / mL.min^{-1}	Minimum / mL.min^{-1}	Minimum / %	Maximum / %
4.00	3.86	3.89	3.83	-4.30	-2.88
3.00	2.89	2.96	2.71	-9.83	-1.20
2.00	2.11	2.15	2.08	4.15	7.45

Table S17. Flow rate and pulsation characterisation monitored using a Coriolis mass flow meter for the annular gear pump at 2, 3 and 4 mL/min flowing toluene through 1/16” PEEK tubing at 25 °C under open-air atmospheric pressure.

Annular gear pump (c)						
Flow rate / mL.min^{-1}	Mean / mL.min^{-1}	Maximum / mL.min^{-1}	Minimum / mL.min^{-1}	Minimum / %	Maximum / %	Frequency / Hz
4.00	4.15	4.18	4.13	3.13	4.40	0.02
3.00	3.07	3.08	3.06	1.93	2.77	0.04
2.00	2.01	2.03	2.00	-0.15	1.50	0.08

Table S18. Flow rate and pulsation characterisation monitored using a Coriolis mass flow meter for the mini annular gear pump at 2, 3 and 4 mL/min flowing toluene through 1/16” PEEK tubing at 25 °C under open-air atmospheric pressure.

Mini annular gear pump (c)				
Mean / mL.min^{-1}	Maximum / mL.min^{-1}	Minimum / mL.min^{-1}	Minimum / %	Maximum / %
4.06	4.07	4.01	0.29	1.72
3.05	3.05	3.06	1.98	1.54
2.01	2.03	2.00	-0.15	1.50

Table S19. Flow rate and pulsation characterisation monitored using a Coriolis mass flow meter for the rotary tetra-piston pump at 2 and 4 mL/min flowing toluene through 1/16” PEEK tubing at 25 °C under open-air atmospheric pressure.

Rotary tetra-piston pump (b)				
Mean / mL.min^{-1}	Maximum / mL.min^{-1}	Minimum / mL.min^{-1}	Minimum / %	Maximum / %
3.81	3.83	3.80	-5.02	-4.38
1.94	1.96	1.93	-3.7	-2.00

11.0 References

1. Vapourtec SF-10 pump, https://www.vapourtec.com/products/sf-10-pump-features/, (accessed 20/05/2021).
2. AZURA P 4.1S, https://www.knauer.net/en/compact-pump-with-pressure-sensor-and-10-mlmin-ceramic-pump-head/p18803, (accessed 20/05/2021).
3. Mikrosysteme GmbH Mzr-6355 HNP https://www.hnp-mikrosysteme.de/en/products/detail/mzr-6355/, (accessed 20/05/021).
4. Mikrosysteme GmbH Mzr-2921X1-hs-vb https://www.hnp-mikrosysteme.de/en/products/detail/mzr-2921x1/, (accessed 20/05/2021).
5. Tacmina QI-10-6T https://www.tacmina.com/products/pump/smoothflow/q_spec.html, (accessed 20/05/2021).
6. Masterflex Single-Syringe Infusion Pump, https://www.coleparmer.co.uk/i/masterflex-single-syringe-infusion-pump-230-vac/7490005, (accessed 20/05/2021).
7. Vici M6 HP https://www.vici.com/liqhand/m6.php, (accessed 20/05/2021).
8. Chemical Resistance of PEEK and Other Polymers, https://www.vici-jour.com/support/resistance.php#:~:text=PEEK%20is%20compatible%20with%20almost,may%20cause%20swelling%20in%20PEEK, (accessed 20/05/2021).
9. G. O. Brown, in *Environmental and Water Resources History*, ed. A. J. F. Jerry R. Rogers, American Society Civil Engineers, Washington, D.C., 2004, vol. 38, ch. 4, pp. 34-43.
10. I. Swan, M. Reid, P. W. A. Howe, M. A. Connell, M. Nilsson, M. A. Moore and G. A. Morris, *J. Magn. Reson.*, 2015, **252**, 120-129.
11. Convective Heat Transfer, https://www.thermopedia.com/content/660/, (accessed 25/05/2021).
12. Conduction in the Cylindrical Geometry, https://web2.clarkson.edu/projects/subramanian/ch330/notes/Conduction%20in%20the%20Cylindrical%20Geometry.pdf, (accessed 25/05/2021).
13. Heat transfer in Flow Through Conduits, https://lin-web.clarkson.edu/projects/subramanian/ch330/notes/Heat%20Transfer%20in%20Flow%20Through%20Conduits.pdf, (accessed 25/05/2021).
14. Tubes, single-phase heat transfer in https://www.thermopedia.com/content/1219/, (accessed 25/05/2021).
15. Heating Systems Flow Rates, https://www.engineeringtoolbox.com/water-flow-rates-heating-systems-d_659.html, (accessed 25/05/2021).
16. ArmaFlex® LTD, https://local.armacell.com/fileadmin/cms/uk/products/en/ArmaflexLTDRangeUKROI.pdf, (accessed 25/05/2021).
17. Polyetheretherketone (PEEK) Material Information, http://www.goodfellow.com/A/Polyetheretherketone.html, (accessed 25/05/2021).
18. FEP Properties, https://www.fluorotherm.com/technical-information/materials-overview/fep-properties/, (accessed 20/05/2021).
19. Parameters for Common Solvents, http://ion.chem.usu.edu/~sbialkow/Research/Tablevalues.html, (accessed 25/05/2021).
20. I. Verein Deutscher, *VDI-Wärmeatlas : Berechnungsblätter für den Wärmeübergang*, VDI-Verlag, Düsseldorf, 8th edn., 1991.

21. Properties of mixture Water/Glycol, https://detector-cooling.web.cern.ch/data/Table%208-3-1.htm, (accessed 25/05/2021).
22. O. Levenspiel, *Chemical Reaction Engineering*, Wiley, Danvers, 3rd edn., 1998.
23. H. S. Fogler, *Elements of chemical reaction engineering*, Prentice Hall, New Jersey, 3rd edn., 1999.
24. H. S. Fogler, *Essentials of Chemical Reaction Engineering*, Pearson, New York, 2nd edn., 2010.
25. A. E. Rodrigues, *Chem. Eng. Sci.*, 2021, **230**, 116188-116188.
26. D. R. Albert, *J. Chem. Educ.*, 2020, **97**, 1491-1494.
27. W. Zhao, *Appl. Math. Model.*, 2021, **92**, 447-465.